



HAL
open science

Energetically consistent Eddy-Diffusivity Mass-Flux schemes for Atmospheric and Oceanic Convection

Manolis Perrot, Florian Lemarié

► **To cite this version:**

Manolis Perrot, Florian Lemarié. Energetically consistent Eddy-Diffusivity Mass-Flux schemes for Atmospheric and Oceanic Convection. 2024. hal-04439113v2

HAL Id: hal-04439113

<https://hal.science/hal-04439113v2>

Preprint submitted on 6 Feb 2024

HAL is a multi-disciplinary open access archive for the deposit and dissemination of scientific research documents, whether they are published or not. The documents may come from teaching and research institutions in France or abroad, or from public or private research centers.

L'archive ouverte pluridisciplinaire **HAL**, est destinée au dépôt et à la diffusion de documents scientifiques de niveau recherche, publiés ou non, émanant des établissements d'enseignement et de recherche français ou étrangers, des laboratoires publics ou privés.



Distributed under a Creative Commons Attribution - NonCommercial 4.0 International License

Energetically consistent Eddy-Diffusivity Mass-Flux schemes for Atmospheric and Oceanic Convection

M. Perrot^{1,*}, F. Lemarié¹

¹Univ Grenoble Alpes, Inria, CNRS, Grenoble INP, LJK, Grenoble, France

Key Points:

- An Eddy-Diffusivity Mass-Flux parameterization is carefully derived from first principles, making the underlying assumptions explicit
- Closed energy budgets between resolved and subgrid energy reservoirs are outlined, including a new formulation of vertical TKE transport
- Comparisons with Large Eddy Simulations show that the new scheme successfully reproduces TKE and its vertical transport

Corresponding author: Manolis Perrot, manolis.perrot@univ-grenoble-alpes.fr

Abstract

A convective vertical mixing scheme rooted in the Eddy-Diffusivity Mass-Flux (EDMF) approach is carefully derived from first principles. This type of closure involves separating vertical turbulent fluxes into two components: an eddy-diffusivity (ED) term that addresses local small-scale mixing in a near isotropic environment, and a mass-flux (MF) transport term that accounts for the non-local transport performed by vertically coherent plumes within the environment. Using the multi-fluid averaging underlying the MF concept, we present consistent energy budgets between resolved and subgrid scales for seawater and dry atmosphere. We show that when using an EDMF scheme, closed energy budgets can be recovered if: (i) bulk production terms of turbulent kinetic energy (TKE) by shear, buoyancy and transport include MF contributions; (ii) boundary conditions are consistent with EDMF, to avoid spurious energy fluxes at the boundary. The performance of the energetically consistent EDMF scheme is evaluated against Large Eddy Simulations (LES) and observational data of oceanic convection. Notably, energetic consistency is key to obtaining accurate TKE and turbulent transport of TKE profiles when compared to LES data. Throughout the theoretical development of the scheme, we maintain transparency regarding underlying assumptions and systematically assess their validity in the light of LES data.

Plain Language Summary

In Earth system models, various important processes occur on scales that are too fine to be resolved with usual grid resolutions. Parameterizations have to be used to approximate the average effect of such processes on the scales resolved by a numerical model. The general objective of the proposed work is to approach the parameterization problem for boundary-layer turbulence and convective plumes in a “consistent” manner. Here the notion of consistency integrates various aspects: global energetic consistency, consistency with a particular averaging technique for the scale-separation, and the rigorous reduction of a physical system to a scale-aware parametric representation based on well-identified and justifiable approximations and hypotheses. An originality is to jointly consider energy budgets including a subgrid energy reservoir on top of the resolved energies allowing the proper coupling between the parameterization and the resolved fluid dynamics. This research is fundamental to obtain an apt representation of mean fields and higher-order turbulent moments and to pave the way toward an alternative methodology to parameterize oceanic convection across scales. Numerical simulations demonstrate the adequacy of the proposed parameterization.

1 Introduction**1.1 Convection in the ocean and atmosphere and its parameterization in numerical models**

Boundary layer convection occurs in the atmosphere and the ocean due to buoyancy fluxes at the surface, which trigger gravitational instabilities. Buoyant plumes then tend to overturn and mix the fluid. When looking at the mean properties of the fluid, it leads to the formation of a well-mixed layer. The accurate representation of such boundary layers is of paramount importance for short-term forecasts as well as for climate projections in the atmosphere (Bony et al., 2015; Schneider et al., 2017) and the ocean (Martin et al., 2013; Piron et al., 2016; Moore et al., 2015; Fox-Kemper et al., 2019). Regarding current computational capacities, plumes are still unresolved in regional and global numerical models, and thus their effects require parameterization. Moreover in ocean modeling, beyond the requirement in terms of grid resolution, hydrostatic equations used in the overwhelming majority of regional and global studies are not suitable for resolving convective phenomena explicitly (Marshall et al., 1997).

61 For any quantity X , standard turbulent mixing models are based on the closure
 62 of vertical turbulent fluxes $\overline{w'X'}$ proportional to the local mean gradient in the form $-K_X\partial_z\overline{X}$
 63 (which corresponds to the so-called Eddy-Diffusivity (ED) closure). Such a closure leads
 64 to a diffusion of \overline{X} , which is often justified by considering that turbulent fluctuations re-
 65 semble Brownian motion (Vallis, 2017; Resseguier et al., 2017). Although the ED clo-
 66 sure has been widely used in many industrial and geophysical applications, it is known
 67 to potentially predict incorrectly higher order moments and even mean fields for com-
 68 plex flows (e.g. Schmitt, 2007). For instance, the inadequacy of ED closures for atmo-
 69 spheric convection has long been highlighted (Deardorff, 1966). Indeed fluctuations are
 70 carried by non-local structures, the buoyant plumes, that can be coherent over the whole
 71 mixed layer. In particular, in such a layer, mean gradients are close to zero ($\partial_z\overline{X} \simeq 0$)
 72 while transport is ensured at leading order by non-zero vertical fluxes $\overline{w'X'}$ which may
 73 even be up-gradient. Indeed, using the assumption of a mixed-layer $\partial_z\overline{X} \simeq 0$ into a tur-
 74 bulent transport equation of the type $\partial_t\overline{X} + \partial_z\overline{w'X'} = 0$ implies that $\overline{w'X'}$ varies lin-
 75 earlyly with z . Such linear variation of fluxes in the mixed layer is well-supported by ob-
 76 servations and numerical experiments (Garratt, 1994b; Denbo & Skyllingstad, 1996).

77 To circumvent ED hypothesis, Deardorff (1966) proposed to introduce a constant
 78 non-local term γ_X in the form $\overline{w'X'} = -K_X(\partial_z\overline{X} - \gamma_X)$. Later on, such a formula-
 79 tion has been refined, where both K_X and γ_X were prescribed by a self-similar profile
 80 function depending on external characteristics of the boundary layer such as surface forc-
 81 ing, stratification at the atmospheric top (or oceanic base) of the mixed layer and im-
 82 plicitly defined mixed layer height (see Troen and Mahrt (1986); Holtslag and Moeng
 83 (1991) for atmospheric models, Large et al. (1994) for oceanic models). This approach
 84 is still in use in some present-day ocean models (e.g. via the CVMIX library, Van Roekel
 85 et al., 2018). Furthermore, in the context of ocean models, two other types of convec-
 86 tive parameterization are sometimes used: (i) a buoyancy sorting scheme (a.k.a. adjust-
 87 ment scheme or non-penetrative scheme), in which static instabilities are eliminated in
 88 one time-step by mixing downward neighboring vertical levels until a neutral buoyancy
 89 profile is attained (e.g. Madec et al., 1991) (ii) an enhanced eddy-viscosity scheme in
 90 which the vertical diffusivity coefficient is artificially increased to a high value as soon
 91 as static instabilities are found on the density profiles. These two approaches are not grounded
 92 on a physical derivation.

93 The present work builds on the combined Eddy-Diffusivity and Mass-Flux (EDMF)
 94 parameterization schemes (Hourdin et al., 2002; Soares et al., 2004). The ED compo-
 95 nent aims to represent turbulent transport in a nearly isotropic environment, in which
 96 convective plumes -modeled by MF terms- support a non-local advective transport. The
 97 MF concept was originally introduced in the atmospheric context to represent deep con-
 98 vective clouds (Arakawa & Schubert, 1974), then it has been adapted to represent shal-
 99 low and dry boundary layer convection in combination with ED schemes. It is intrin-
 100 sically based on a multi-fluid averaging (Yano, 2014; Thuburn et al., 2018) of the fluid
 101 equations. In ocean models the EDMF concept has been first introduced by Giordani
 102 et al. (2020), and has been gaining increasing attention (e.g. Garanaik et al. (2024), or
 103 a recent implementation in Oceananigans, Ramadhan et al. (2020)).

104 1.2 Parameterization development and physics dynamics coupling

105 The general objective of the proposed work is to approach the parameterization
 106 problem in a “consistent” manner. Here the notion of consistency integrates various as-
 107 pects: consistency with the laws of physics, energetic consistency at both continuous (e.g.
 108 Eden, 2016; Jansen et al., 2019; Eden & Olbers, 2014) and discrete (e.g. Burchard, 2002)
 109 levels, consistency with a particular choice of scale-separation operator (Higgins et al.,
 110 2013; Lauritzen et al., 2022), and the rigorous reduction of a physical system to a scale-
 111 aware parametric representation based on well-identified approximations and hypothe-
 112 ses (Honnert et al., 2016; Tan et al., 2018).

113 Regarding boundary layer parameterizations, eddy-diffusivity intensity often scales
 114 with the turbulent kinetic energy (TKE) which is computed via a parameterized prog-
 115 nostic equation. TKE represents a subgrid kinetic energy that exchanges energy with
 116 the resolved reservoirs. The use of mass-flux terms leads to energy transfers and redis-
 117 tributions that must be taken into account in the TKE equation to ensure energetic consistency
 118 between resolved and subgrid scales. In addition, the boundary conditions of
 119 the mass-flux equations must be consistent between ED and MF to avoid double-counting
 120 and artificial energy fluxes at the fluid boundary. Apart from a brief discussion in Tan
 121 et al. (2018) for unsteady plume models, the energetically consistent coupling of TKE
 122 and standard EDMF schemes has not been, to our knowledge, discussed in the litera-
 123 ture. Some modifications of the TKE equation when using a mass-flux model have been
 124 proposed for the buoyancy production term (Witek et al., 2011b) and the vertical tur-
 125 bulent transport of TKE (Witek et al., 2011a; Han & Bretherton, 2019). However, these
 126 studies are not motivated by considerations of energetic consistency.

127 1.3 Goals and organisation of the paper

128 The aim of this paper is two-fold. First, we intend to provide an introductory, self-
 129 contained, and pedagogical derivation of EDMF schemes starting from first principles,
 130 to guide consistency considerations. Second, we derive theoretical energy budgets and
 131 provide guidelines to obtain energetically consistent EDMF models. Consequently, this
 132 paper is intended to both the oceanographic community as a pedagogical introduction
 133 to EDMF, and the atmospheric community seeking to reduce energy biases in EDMF
 134 models. The paper is organized as follows. In section 2, we expose the derivation of an
 135 EDMF scheme from first principle, systematically discuss the successive assumptions at
 136 stake, provide closures according to state-of-the-art practice, and discuss consistent bound-
 137 ary conditions. In section 3, we recall the theoretical resolved and subgrid energy bud-
 138 gets of a horizontally averaged Boussinesq fluid without closures. In section 4, we ex-
 139 pose the necessary modification of the parameterized turbulent kinetic energy (TKE)
 140 equation to obtain closed energy budgets when using EDMF. Furthermore, we derive ver-
 141 tically averaged energy budgets to reveal the role of boundary conditions on the energy
 142 fluxes. In section 5, we analyze the assumptions used in the derivation of the scheme in
 143 light of data from Large Eddy Simulation (LES) of idealized oceanic deep convection.
 144 Then we evaluate the energetically consistent EDMF scheme against such data, and against
 145 realistic data of oceanic deep convection events in the Mediterranean Sea. In appendices,
 146 we provide discretization details for interested model developers and energy budgets in
 147 the anelastic setting which are more commonly used by the atmospheric community.

148 2 Derivation of EDMF scheme

149 2.1 Formal derivation

150 We start from the unaveraged Navier-Stokes equations under the Boussinesq as-
 151 sumption in a cubic domain $L_x \times L_y \times H$:

$$\nabla \cdot \mathbf{u} = 0 \quad (1)$$

$$\partial_t \mathbf{u} = -\nabla \cdot (\mathbf{u} \otimes \mathbf{u}) - \frac{1}{\rho_0} \nabla p^\dagger + b \mathbf{e}_z + \nu \nabla^2 \mathbf{u} \quad (2)$$

$$\partial_t \phi = -\nabla \cdot (\phi \mathbf{u}) + S_\phi \quad (3)$$

$$b = b_{\text{eos}}(\phi) \quad (4)$$

152 where $\mathbf{u} = (u, v, w)$ denotes the velocity field in a local Cartesian frame of reference $(\mathbf{e}_x, \mathbf{e}_y, \mathbf{e}_z)$,
 153 z ranges from 0 to H in the atmosphere and $-H$ to 0 in the ocean, ρ_0 is a constant refer-
 154 ence density, the pressure has been decomposed as $p = p_{\text{ref}}(z) + p^\dagger(x, y, z, t)$ with
 155 $\partial_z p_{\text{ref}} = -\rho_0 g$, b is the buoyancy acceleration, ϕ is any entropic variable describing each
 156 component of the fluid, S_ϕ is an additional source term (typically molecular diffusion).

157 For instance, in the context of a dry atmosphere modeled as an ideal gas, a simple choice¹
 158 would be $\phi = \theta$, where θ is the potential temperature, and $b_{\text{eos}}(\theta) = g(\theta - \theta_0)/\theta_0$. In
 159 the context of ocean dynamics, one would choose conservative temperature and salin-
 160 ity ($\phi = \theta, S$) and a linear equation of state, $b_{\text{eos}}(\theta, S) = g\alpha(\theta - \theta_0) - g\beta(S - S_0)$ where
 161 α and β are thermal expansion and haline contraction coefficients, respectively, and θ_0
 162 and S_0 are reference temperature and salinity. Details on source terms S_ϕ are given in
 163 section 3. For the sake of simplicity, we do not include the Coriolis term in the present
 164 study. Since the Coriolis force is energetically-neutral it does not interfere with the deriva-
 165 tions made throughout this paper. Next, we explicit the framework in which vertical mix-
 166 ing parameterizations are usually developed. We adopt a semi-discrete approach, where
 167 the *horizontal* fluid domain is divided into a $N_x \times N_y$ mesh. Each horizontal grid cell
 168 has length Δx_i and width Δy_j , and we denote (x_i, y_j) its center. Note that the time and
 169 vertical coordinates z are kept *continuous*. The spatial domain can be thought of $N_x \times$
 170 N_y vertical columns stacked together. In a numerical model discretized on such a mesh,
 171 the computed variables would be interpreted in a finite volume approach (LeVeque, 2002).
 172 For any field $X = \mathbf{u}, \phi \dots$ one can define the following horizontal average and fluctua-
 173 tion

$$\bar{X}(x_i, y_j, z, t) := \frac{1}{\Delta x_i \Delta y_j} \int_{\Delta x_i \times \Delta y_j} X(x, y, z, t) dx dy, \quad X' = X - \bar{X}$$

174 If we recast (1)–(3) in the generic form $\partial_t X + \nabla \cdot (\mathbf{u}X) = S_X$, and then apply such a
 175 horizontal average, we obtain

$$\partial_t \bar{X} + \partial_z (\bar{w}\bar{X} + \overline{w'X'}) + \frac{1}{\Delta x_i \Delta y_j} \oint_{\partial(\Delta x_i \times \Delta y_j)} X \mathbf{u}_h \cdot d\mathbf{n} = \bar{S}_X \quad (5)$$

176 where $\mathbf{u}_h = (u, v, 0)$ denotes the horizontal velocity vector and $d\mathbf{n}$ is an outward point-
 177 ing line integral element, i.e. $\mathbf{u}_h \cdot d\mathbf{n} = udy - vdx$. The boundary integral in (5) is the
 178 total (resolved and subgrid) horizontal flux of X . In a numerical model, \bar{X} would be in-
 179 terpreted as the resolved variable, X' would be an unresolved fluctuation, the precise form
 180 of the horizontal flux would depend on the numerical scheme (and possibly on param-
 181 eterizations), and the vertical subgrid flux $\overline{w'X'}$ has to be closed by a parameterization.
 182 When focusing on the parameterization of vertical mixing processes, it is common to con-
 183 ceptually isolate one vertical column of fluid to work with a one-dimensional Single-Column
 184 Model (SCM) (e.g. Zhang et al., 2016). Any quantity is assumed statistically invariant
 185 along the horizontal direction, meaning that in practice the horizontal fluxes and pres-
 186 sure gradients are neglected. We further simplify the problem with two additional as-
 187 sumptions: First, the bottom of the column is considered flat. Along with a non-penetration
 188 condition, this leads to $\bar{w}(z = 0) = 0$. Now the averaged volume conservation under
 189 the horizontal homogeneity $\partial_z \bar{w} = 0$ implies that $\bar{w}(z) = 0$ at any level z . Second, in
 190 the vertical momentum budget, the momentum flux divergence $\partial_z \overline{w'w'}$ is neglected, lead-
 191 ing to the hydrostatic approximation $\partial_z \bar{p}^\dagger = b$. The SCM equations are then

$$\partial_t \bar{\mathbf{u}}_h = -\partial_z \overline{w' \mathbf{u}'_h} \quad (6)$$

$$\partial_t \bar{\phi} = -\partial_z \overline{w' \phi'} + \bar{S}_\phi \quad (7)$$

192 where the molecular viscosity can be safely neglected in the mean momentum budget.
 193 The remainder of this article will use these SCM assumptions, and indices i, j will be dropped.
 194 For readers interested in the inclusion of horizontal fluxes, we refer them to Yano (2014)
 195 and Tan et al. (2018). As an alternative to the semi-discrete description presented above,

¹ In both oceanic and atmospheric context, we use simple thermodynamic descriptions allowing convec-
 tion. Although these descriptions are inaccurate for real-world applications, they are sufficient to expose
 how to build energetically consistent EDMF parameterizations. Energy budgets for the anelastic approxi-
 mation can be found in Appendix E

196 a fully continuous description can be carried out by replacing the horizontal average by
 197 smoothing kernels on the scale of the grid size (see for example Thuburn et al. (2018)
 198 in the context of mass-flux schemes).

199 We now *assume* a formal decomposition of the horizontal column area $\Delta x \times \Delta y$
 200 into two horizontal subdomains of areas $\mathcal{A}_e(z, t)$ and $\mathcal{A}_p(z, t)$ which also depend on depth
 201 and time. Such decomposition is meant to isolate the coherent convective structures usu-
 202 ally referred to as *plumes* (occupying the subdomain of area $\mathcal{A}_p(z, t)$) from the rest of
 203 the flow, referred to as the *environment* (occupying the subdomain of area $\mathcal{A}_e(z, t)$). We
 204 introduce the following notations to characterize the subdomain averaged field and *frac-*
 205 *tional* area (for $i = e, p$):

$$\begin{aligned} X_i &= \frac{1}{\mathcal{A}_i(z, t)} \int_{\mathcal{A}_i(z, t)} X(x, y, z, t) dx dy \\ a_i &= \mathcal{A}_i(z, t) / (\Delta x \times \Delta y) \end{aligned}$$

206 Any mean field can then be decomposed as

$$\bar{X} = a_e X_e + a_p X_p$$

207 In particular, when $X \equiv 1$ we get the constraint $a_e = 1 - a_p$. After some algebra, any
 208 turbulent flux can be recast as

$$\overline{w'X'} = a_e \overline{w'_e X'_e} + a_p \overline{w'_p X'_p} + a_e (w_e - \bar{w})(X_e - \bar{X}) + a_p (w_p - \bar{w})(X_p - \bar{X}) \quad (8)$$

209 where

$$\overline{w'_i X'_i} = \frac{1}{\mathcal{A}_i(z, t)} \int_{\mathcal{A}_i(z, t)} (X - X_i)(w - w_i) dx dy$$

210 For each subdomain, the $a_i(w_i - \bar{w})(X_i - \bar{X})$ terms in (8) account for the "mass-flux"
 211 (i.e. the contribution of coherent structures to the flux), whereas the $a_i \overline{w'_i X'_i}$ terms are
 212 a contribution from internal variability. Applying the subdomain average to any conser-
 213 vation law of the form $\partial_t X + \nabla \cdot (\mathbf{u}X) = S_X$ and using Reynolds transport theorem
 214 leads to (see appendix A of Tan et al. (2018) and Yano (2014) for full derivation)

$$\partial_t(a_i X_i) + \partial_z \left(a_i w_i X_i + a_i \overline{w'_i X'_i} \right) + \frac{1}{\mathcal{A}_i} \oint_{\partial \mathcal{A}_i} X \mathbf{u}_r \cdot d\mathbf{n} = a_i S_{X,i} \quad (9)$$

215 where the relative horizontal boundary velocity is $\mathbf{u}_r = \mathbf{u}_h - \partial_t \mathbf{r}_b - w \partial_z \mathbf{r}_b$ and $\mathbf{r}_b =$
 216 $(x_b(z, t), y_b(z, t))$ is the position vector of boundary elements. The three terms that con-
 217 sstitute \mathbf{u}_r indicate that boundary fluxes can arise respectively due to horizontal veloc-
 218 ity across the boundary, to (apparent) horizontal velocity of the boundary, or to verti-
 219 cal velocity if the boundary of the 3D plume is vertically tilted (i.e. $\partial_z \mathbf{r}_b \neq 0$).

220 2.2 Standard assumptions

221 2.2.1 Plume-Environment decomposition

222 The first standard assumption we have already made is to consider only two sub-
 223 domains, the convective plume and the environment. This is justified since in convec-
 224 tive situations the main contribution to the fluxes comes from the plumes. However, the
 225 framework is flexible enough to incorporate an arbitrary number of components. In par-
 226 ticular, several studies of the atmospheric convective boundary layer (CBL) underline
 227 the importance of returning coherent structures around the plumes, often referred to as
 228 CBL downdrafts (Schmidt & Schumann, 1989; Couvreux et al., 2007; Brient et al., 2023).

229 2.2.2 Entrainment/Detrainment and Upstream approximation

230 Net fluid exchange at the horizontal boundary of the plume domain can be further
 231 decomposed into fluid *entrained* into the plume from the environment, and fluid *detrained*

232 out of the plume into the environment, namely

$$\begin{aligned} \frac{1}{\mathcal{A}_p} \oint_{\partial\mathcal{A}_p} \mathbf{u}_r \cdot d\mathbf{n} &= \frac{1}{\mathcal{A}_p} \oint_{\partial\mathcal{A}_p, \mathbf{u}_r \cdot \mathbf{n} > 0} \mathbf{u}_r \cdot d\mathbf{n} + \frac{1}{\mathcal{A}_p} \oint_{\partial\mathcal{A}_p, \mathbf{u}_r \cdot \mathbf{n} < 0} \mathbf{u}_r \cdot d\mathbf{n} \\ &= D - E \end{aligned}$$

233 where $E(> 0)$ is called *entrainment rate* and $D(> 0)$ is called *detrainment rate*. We fur-
 234 ther assume that the value of X at the boundary is either equal to the mean value in
 235 the environment when entrainment is occurring, or the mean value in the plume when
 236 detrainment is occurring. This is the so-called *upstream approximation*, formulated as²

$$\frac{1}{\mathcal{A}_p} \oint_{\partial\mathcal{A}_p} X \mathbf{u}_r \cdot d\mathbf{n} = X_e E - X_p D \quad (10)$$

237 As a result of this approximation, the plume equation reads

$$\partial_t(a_p X_p) + \partial_z(a_p w_p X_p) = -\partial_z(a_p \overline{w'_p X'_p}) + E X_e - D X_p + a_p S_{X,p} \quad (11)$$

238 In particular when $X \equiv 1$, we get the plume area conservation equation:

$$\partial_t a_p + \partial_z(a_p w_p) = E - D \quad (12)$$

239 2.2.3 Steady plume hypothesis

240 A common hypothesis is that the plume domain is in a quasi-steady regime, thus
 241 neglecting the temporal tendency compared to vertical advection. The relevance of this
 242 hypothesis is numerically tested using idealized cases in section 5.3. An *a priori* scal-
 243 ing estimation can also be performed. Introducing τ , h , and W the characteristic time,
 244 depth, and vertical velocity scales of the plume, the order of magnitude of the ratio be-
 245 tween the temporal tendency and vertical advection can be estimated as follows

$$O\left(\frac{\partial_t(a_p X_p)}{\partial_z(a_p w_p X_p)}\right) = \frac{h/\tau}{W} \simeq \frac{w_{\text{ent}}}{W} \quad (13)$$

246 where $w_{\text{ent}} = \frac{d}{dt}h$ is the boundary layer vertical entrainment velocity. In the limit of
 247 free convection triggered by a surface buoyancy loss $B_0 < 0$ into a fluid of constant strat-
 248 ification N_0^2 , the classical convective scalings $h \propto \sqrt{-B_0/N_0^2 t}$ and $W = (-B_0 h)^{1/3}$
 249 (Turner, 1979; Deardorff, 1970) lead to

$$\frac{w_{\text{ent}}}{W} \propto \frac{1}{(N_0 t)^{2/3}} \quad (14)$$

250 In a different context, that of the development of a shear-driven mixed layer forced by
 251 surface wind stress $\rho_0 u_*^2$, Kato and Phillips (1969) showed that $w_{\text{ent}}/u_* \propto u_*^2/N_0^2 h$. In
 252 such a layer $W \simeq u_*$, leading to a scaling similar to (14). These scalings suggest that
 253 as long as the surface forcings (represented here by u_* and B_0) are evolving slowly com-
 254 pared to $1/N_0$, the steady plume hypothesis remains valid. Under such a hypothesis, the
 255 plume equation for any field X now reads

$$\partial_z(a_p w_p X_p) = -\partial_z(a_p \overline{w'_p X'_p}) + E X_e - D X_p + a_p S_{X,p} \quad (15)$$

256 As a summary, we rewrite the coupled resolved/plume system in an advective form us-
 257 ing area conservation and $\overline{X} = (1 - a_p)X_e + a_p X_p$:

$$\partial_t \overline{X} = -\partial_z \overline{w' X'} + \overline{S}_X \quad (16)$$

$$\overline{w' X'} = \frac{1}{1 - a_p} a_p w_p (X_p - \overline{X}) + (1 - a_p) \overline{w'_e X'_e} + a_p \overline{w'_p X'_p} \quad (17)$$

$$a_p w_p \partial_z X_p = -\frac{1}{1 - a_p} E (X_p - \overline{X}) - \partial_z(a_p \overline{w'_p X'_p}) + a_p S_{X,p} \quad (18)$$

² In the context of 3D models, the plume boundary $\partial\mathcal{A}_p$ can cross the horizontal boundary of the grid cell. The corresponding contribution to the integral can be interpreted as a resolved flux divergence across the grid cell, namely $\nabla_h \cdot (a_p \mathbf{u}_{h,p} X_p + a_p \overline{\mathbf{u}'_{h,p} X'_p})$ (see section 5.1 of Yano (2014)).

258 Several authors have recently proposed to relax the steady plume hypothesis (Tan et al.,
 259 2018; Thuburn et al., 2018). However, the overwhelming majority of mass flux schemes
 260 implemented in realistic models considers a plume domain in a quasi-steady regime.

261 **2.2.4 Small area limit**

262 A last standard hypothesis is that the fractional area of the plume is *small* com-
 263 pared to that of the environment (see section 5.3 for a direct evaluation against LES).
 264 This generally means considering the formal limit $a_p \rightarrow 0$ and $a_e \rightarrow 1$ in the previous
 265 equations while keeping non-zero mass-flux $a_p w_p$ and source terms. Yano (2014) proposes
 266 to assume $a_p w_p = O(w_e)$ and $a_p S_{X,p} = O(S_{X,e})$ to retain an order one contribution
 267 of $a_p w_p (X_p - \bar{X})$ in (17), and to keep an order one contribution of advection and forc-
 268 ings in (18). In the small area limit, any environmental field X_e (except w_e) can be ap-
 269 proximated by the mean field, the vertical turbulent flux (17) becomes

$$\overline{w'X'} = a_p w_p (X_p - \bar{X}) + \overline{w'_e X'_e} \quad (19)$$

270 and the plume equation (18) now reads

$$a_p w_p \partial_z X_p = -E(X_p - \bar{X}) + a_p S_{X,p} \quad (20)$$

271 In the remainder of this study, we will adopt such a small area limit. Noteworthy is the
 272 effort by some authors to relax this hypothesis to explore the "grey zone" of atmospheric
 273 turbulence or to devise scale-aware parameterization schemes when the grid is refined
 274 to the point where a_p is no longer small (Honnert et al., 2016; Tan et al., 2018). For the
 275 sake of completeness, we include in Appendix A the system of plume equations obtained
 276 when relaxing the small area limit while still neglecting subplume fluxes $\overline{w'_p X'_p}$ (in line
 277 with Tan et al. (2018)). This system only deviates by factors $1/(1-a_p)$ from the "small-
 278 area" system, making it simple to implement in practice.

279 *Remark:* To our knowledge, the interplay between the small area limit and the steady
 280 plume hypothesis has been only discussed in Yano (2014) where the author argues that
 281 the formal limit $a_p \rightarrow 0$ implies $\partial_t(a_e X_e) \rightarrow \partial_t \bar{X}$, and thus recovers the steady-plume
 282 hypothesis $\partial_t(a_p X_p) \rightarrow 0$ using (8). Using such formal limit and $a_p w_p = O(w_e)$ im-
 283 plies that $w_p \rightarrow \infty$. Since plume properties are advected by w_p , such infinite velocity
 284 assumption is interpreted as an instantaneous adjustment to any surface perturbation,
 285 consistently with the steady-plume hypothesis. Using Yano's scaling, an estimate of the
 286 ratio between temporal tendency and vertical advection is now

$$O\left(\frac{\partial_t(a_p X_p)}{\partial_z(a_p w_p X_p)}\right) = \frac{O(a_p)/\tau}{w_e/h} \rightarrow 0 \text{ if } a_p \rightarrow 0$$

287 which shows that such scaling indeed implies stationarity. However, the alternative scal-
 288 ing we proposed in (13) decouples the small area limit from the stationarity assumption
 289 and is found to be validated in numerical simulations (see 5.3). Moreover, our scaling
 290 analysis seems more general since it merely takes into account scales for each field, with-
 291 out further assumptions, and thus justifies the potential use of stationary equations while
 292 relaxing the small area assumption.

293 **2.3 Standard Closures**

294 Thanks to the assumptions made so far, we have arrived at equations of the gener-
 295 al form (20) for the plume, and (19) for vertical turbulent fluxes. At this stage, addi-
 296 tional closure assumptions are required to express the entrainment and detrainment rates,
 297 the flux $\overline{w'_e X'_e}$, and the pressure gradients appearing in the $S_{w,p}$ and $S_{u_h,p}$ terms.

298 **2.3.1 Plume vertical pressure gradient**

299 Plume vertical pressure gradients are usually parameterized as the combination of
 300 a virtual mass term (e.g. Bretherton et al., 2004) – representing the reduction of plume
 301 buoyancy due to pushing and pulling on the environment –, a reduced entrainment term
 302 and a quadratic drag term. Several formulations have been proposed (see Roode et al.
 303 (2012) for an intercomparison in the context of shallow cumulus convection). In line with
 304 usual practices in the atmospheric context (e.g. Pergaud et al., 2009; Rio et al., 2010)
 305 we consider

$$a_p \left(\frac{1}{\rho_0} \partial_z p^\dagger \right)_p = (a - 1) a_p B_p + (b - 1) (-E w_p) + b' a_p w_p^2 \quad (21)$$

306 leading to the plume vertical momentum budget

$$a_p w_p \partial_z w_p = a a_p B_p - b E w_p - \sigma_o^a b' a_p w_p^2 \quad (22)$$

307 where a , b and b' are positive parameters, $\sigma_o^a = +1$ in the atmosphere and -1 in the
 308 ocean, and $B_p = b_p - \bar{b}$. Note that in the case of dry atmosphere or seawater with a
 309 linearized equation of state, we have $b_p - \bar{b} = b_{\text{eos}}(\phi_p) - b_{\text{eos}}(\bar{\phi})$.

310 **2.3.2 Horizontal momentum budget**

311 Based on the work of Rotunno and Klemp (1982) and Wu and Yanai (1994), Gregory
 312 et al. (1997) proposed a parameterization of the plume horizontal pressure gradient as
 313 an advective correction of the form

$$a_p \left(\frac{1}{\rho_0} \nabla_h p^\dagger \right)_p = a_p w_p C_u \partial_z \bar{\mathbf{u}}_h \quad (23)$$

314 where C_u is a parameter. We show in Section 4.5 that energy cosntraints impose $0 \leq$
 315 $C_u < 1$.

316 **2.3.3 Eddy-Diffusivity closure**

317 The environment is thought of as a subdomain where only small-scale turbulence
 318 occurs, thus supporting the hypothesis of a closure of the vertical flux with an eddy-diffusivity,
 319 $\overline{w'_e X'_e} \underset{\text{ED}}{=} -K_X \partial_z X_e \underset{a_p \ll 1}{\simeq} -K_X \partial_z \bar{X}$. This leads to the eddy-diffusivity mass-flux clo-
 320 sure of subgrid fluxes

$$\overline{w' X'} = \underbrace{-K_X \partial_z \bar{X}}_{\text{ED}} + \underbrace{a_p w_p (X_p - \bar{X})}_{\text{MF}} \quad (24)$$

321 In the present study, the eddy viscosity K_u and diffusivity K_ϕ in turbulent vertical fluxes
 322 are computed from a turbulence closure model based on a prognostic equation for the
 323 turbulent kinetic energy (TKE) $k = \overline{\mathbf{u}' \cdot \mathbf{u}'}/2$ and a diagnostic computation of appropri-
 324 ate length scales (a.k.a. 1.5-order turbulence closure). For the numerical tests in the
 325 oceanic context presented in Sec. 5, we use a formulation close to that of the Nucleus
 326 for European Modelling of the Ocean model (NEMO, Madec et al., 2019). The eddy-
 327 viscosity and diffusivity are classically assumed to be related to TKE by

$$\begin{aligned} K_u &= c_m l_m \sqrt{k} \\ K_\phi &= K_u (\text{Pr}_t)^{-1} \end{aligned}$$

328 with l_m a mixing length scale, Pr_t the non-dimensional turbulent Prandtl number, and
 329 c_m is a constant (further details on the computations of these quantities are given in Ap-
 330 pendix B). Details of the prognostic equation for k , in connection with energetic consi-
 331 stency requirements, are given in Sec. 3. We acknowledge that since ED represents tur-
 332 bulence in the environment, one should use the environmental TKE $1/2 \overline{\mathbf{u}'_e \cdot \mathbf{u}'_e}$ instead
 333 as it is done in Tan et al. (2018). Although no significant effect could be seen in prelimi-
 334 nary idealized numerical tests, this point should be further explored.

$\overline{w'\phi'}$	$= a_p w_p (\phi_p - \bar{\phi}) - K_\phi \partial_z \bar{\phi}$	Vertical turbulent flux for component ϕ
$\overline{w'u'_h}$	$= a_p w_p (\mathbf{u}_{h,p} - \bar{\mathbf{u}}_h) - K_u \partial_z \bar{\mathbf{u}}_h$	Vertical turbulent momentum flux
$\partial_z(a_p w_p)$	$= E - D$	Plume area conservation equation
$a_p w_p \partial_z \phi_p$	$= E(\bar{\phi} - \phi_p)$	Plume equation for component ϕ
$a_p w_p \partial_z \mathbf{u}_{h,p}$	$= E(\bar{\mathbf{u}}_h - \mathbf{u}_{h,p}) + a_p w_p C_u \partial_z \bar{\mathbf{u}}_h$	Plume horizontal momentum equation
$a_p w_p \partial_z w_p$	$= -bEw_p + a_p \{aB_p - \sigma_o^a b'(w_p)^2\}$	Plume vertical velocity equation
B_p	$= b_{\text{eos}}(\phi_p) - b_{\text{eos}}(\bar{\phi})$	Buoyancy forcing term
K_u	$= c_m l_m \sqrt{k}$	Eddy-viscosity
K_ϕ	$= K_u (\text{Pr}_t)^{-1}$	Eddy-diffusivity

Table 1: Summary of the vertical turbulent flux formulation and plume equations in the small area limit under the steady plume hypothesis detailed in sections 2.1, 2.2 and 2.3. The mean terms quantities $\bar{\mathbf{u}}_h$ and $\bar{\phi}$ are the prognostic variables of the model and the equation for k is given in Sec. 4 and in Tab. 2.

2.3.4 Entrainment and detrainment closures

Entrainment and detrainment closures are still a topic of extensive research in the atmospheric modeling community. One difficulty is that a given closure can only be specific to a certain type of convection (de Rooy et al., 2013). To close entrainment and detrainment rates³, we adapt the formulation proposed by Rio et al. (2010), namely

$$E = a_p \beta_1 \max(0, \partial_z w_p) \quad (25)$$

$$D = -a_p \beta_2 \min(0, \partial_z w_p) + \sigma_o^a a_p w_p \delta_0 \quad (26)$$

where the two parameters β_1 and β_2 are positive, δ_0 is a positive minimum detrainment. In order to guarantee $0 \leq a_p \leq 1$, it is sufficient to impose $0 \leq \beta_1 \leq 1$ and $1 \leq \beta_2 < 2$ (see Appendix F).

To summarize the formal derivation made so far, the closure of fluxes and associated plume equations of the resulting EDMF scheme are provided in Tab. 1.

2.4 Consistent boundary conditions for mean and plume equations

2.4.1 General concepts

Under the aforementioned assumptions, the budget equations governing plume quantities simplify into a system of non-linear first-order ordinary differential equations with respect to the variable z . Accordingly, a single boundary condition at $z = 0$ (i.e., the top of the water column or the bottom of the air column depending on the fluid under consideration) is sufficient for the computation of plume variables. At the boundary $z = 0$, consistent boundary conditions for the plume variable X_p and the mean variable \bar{X} must comply with the EDMF flux decomposition (24)

$$\overline{w'X'}(0) = -K_X \partial_z \bar{X}(0) + a_p(0)w_p(0)(X_p(0) - \bar{X}(0)) \quad (27)$$

³ In the literature, closures are usually provided for *fractional* entrainment and detrainment rates, respectively $\epsilon = E/(\sigma_o^a a_p w_p)$ and $\delta = D/(\sigma_o^a a_p w_p)$, where $-a_p w_p$ is the oceanic mass-flux and $+a_p w_p$ is the atmospheric mass-flux.

354 Such a constraint should guide modeling choices concerning boundary conditions. In-
 355 deed, it systematically guarantees the correct partition of surface fluxes, and thus avoids
 356 double-counting biases linked to non-physical energy sources/sinks at the boundary (see
 357 Sec. 4.5). For instance, suppose the values of $\overline{w'X'}(0)$, $a_p(0)$, $w_p(0)$ and $X_p(0)$ are jointly
 358 specified. Then (27) would turn into a Robin (a.k.a type 3) boundary condition for the
 359 \overline{X} equation which arises naturally in advection-diffusion equations (e.g. Hahn and Özişik
 360 (2012), chapter 1-5). At the boundary $z = \sigma_o^a H$, a no-flux condition is imposed for the
 361 mean equation. For the specific case of oceanic convection reaching the ocean bottom,
 362 a possibility is to add a penalization term to ensure the condition $w_p(z = -H) = 0$.

363 2.4.2 Oceanic context

364 For oceanographic applications, we consider that a surface flux $\overline{w'X'}(0)$ is prescribed.
 365 The mass flux component becomes non-zero close to the surface as soon as the entrain-
 366 ment rate (25) is itself non-zero. In this case the conservation of volume reads

$$\partial_z(a_p w_p) = a_p w_p \left(\beta_1 \frac{1}{w_p} \partial_z w_p + \delta_0 \right)$$

367 which can be easily integrated vertically to obtain

$$a_p(z) w_p(z) = (a_p(0) w_p(0)) \left(e^{\delta_0 z} \left(\frac{w_p(z)}{w_p(0)} \right)^{\beta_1} \right)$$

368 As $\beta_1 < 1$, non-trivial solutions are obtained if and only if non-zero boundary values
 369 for a_p and w_p are chosen. In the remainder, we adopt the following simple choice,

$$X_p(0) = \overline{X}(0), \quad a_p(0) = a_p^0, \quad w_p(0) = w_p^0$$

370 where a_p^0 and w_p^0 are parameters. According to (27), it implies that all the surface flux
 371 is allocated in the ED component, as advocated by Tan et al. (2018). This particular choice
 372 of boundary condition is also motivated by the fact that it implies at the discrete level
 373 that convection is triggered as soon as the surface Brünt-Väisälä frequency $\partial_z b(0)$ is neg-
 374 ative (see Appendix F for further details). As a result, (27) turns into the Neumann bound-
 375 ary condition $-K_X \partial_z X(0) = \overline{w'X'}(0)$, which is standard practice for ED-only closures.

376 Alternatively, Soares et al. (2004) proposed that close to the surface, the plume/mean
 377 buoyancy difference B_p should depend on the surface buoyancy flux, leading to

$$b_p(z) = \bar{b}(z) + \beta \frac{\overline{w'b'}(0)}{\sqrt{k(z)}} \quad (28)$$

378 where β is a constant. We show in Appendix C that our formulation is in fact equiva-
 379 lent to (28) for if $\beta = z/(c_b l_b(0))$ and $k(z) \simeq k(0)$. However, when using this type of
 380 boundary condition exactly at the surface (as in Pergaud et al., 2009), special attention
 381 must be paid when providing the ED flux, since the EDMF decomposition (27) imposes

$$-K_b(0) \partial_z \bar{b}(0) = \left(1 - \frac{a_p(0) w_p(0) \beta}{\sqrt{k(0)}} \right) \overline{w'b'}(0)$$

382 which is different from the standard Neumann condition used for ED-only closures.

383 2.4.3 Atmospheric context: consistency with Monin-Obukhov theory

384 For atmospheric applications, boundary conditions for the mean variables are com-
 385 monly imposed using Monin-Obukhov similarity theory (MOST), which assumes that
 386 in a surface layer located between $z = 0$ and $z = z_1$ fluxes are constant, and mean vari-
 387 ables obey a quasi-logarithmic profile. To properly include a surface layer obeying MOST,

388 then the EDMF flux decomposition must be imposed at the new model boundary $z =$
 389 z_1 , namely

$$\overline{w'X'}(z_1) = -K_X(z_1)\partial_z\overline{X}(z_1) + a_p(z_1)w_p(z_1)(X_p(z_1) - \overline{X}(z_1)) \quad (29)$$

390 At this stage, we can point the following ambiguity. When the MF term is non-zero, it
 391 is not clear whether the flux arising from MOST – which is an ED flux – should be al-
 392 located to the ED term $-K_X(z_1)\partial_z\overline{X}(z_1)$, or to the total flux $\overline{w'X'}(z_1)$ using the con-
 393 stant flux assumption. Although not discussed transparently, it seems that the second
 394 option is a common practice. However, in such a case, special attention would be required
 395 to compute the total flux entering in energy budget computations.
 396 Although beyond the scope of this article, we would like to point out that MOST is known
 397 to fail in strongly unstable conditions (Johansson et al., 2001; Li et al., 2018). Recently,
 398 Li et al. (2021) proposed corrections to formulate departure from MOST in the form of
 399 an EDMF closure including updraft *and* downdraft contributions. This approach could
 400 potentially help provide physically consistent boundary conditions to EDMF models.

401 At this stage, we have provided all the elements and underlying assumptions re-
 402 quired to formulate an EDMF-type scheme (see Appendix F for the discretization as-
 403 pects). Before studying the energetic impacts of using MF components, we derive the-
 404oretical horizontally averaged energy budgets.

405 **3 Horizontally Averaged Energy budgets**

406 The total specific energy E_{tot} of the fluid is the sum of the mean kinetic energy $E_k =$
 407 $(\overline{\mathbf{u}_h \cdot \mathbf{u}_h})/2$, the turbulent kinetic energy $k = (\overline{\mathbf{u}' \cdot \mathbf{u}'})/2$, the potential energy $E_p = gz$
 408 and the mean internal energy E_i . In the following sections, we recall the expression of
 409 these energy reservoirs under the Boussinesq approximation, and we derive budgets for
 410 each of these reservoirs, regardless of flux parameterization. For completeness, energy bud-
 411 gets for anelastic models of dry atmosphere are derived in Appendix E.

412 **3.1 Kinetic energies**

413 Under the SCM assumptions exposed in Sec. 2.1, we can derive budgets for the re-
 414 solved kinetic energy E_k and the turbulent kinetic energy k :

$$\partial_t E_k + \partial_z T_{E_k} = \overline{w'\mathbf{u}'_h} \cdot \partial_z \overline{\mathbf{u}_h} \quad (30)$$

$$\partial_t k + \partial_z T_k = -\overline{w'\mathbf{u}'_h} \cdot \partial_z \overline{\mathbf{u}_h} + \overline{w'b'} - \overline{\epsilon}_\nu \quad (31)$$

415 where $\overline{\epsilon}_\nu = \nu \overline{\partial_z \mathbf{u}' \cdot \partial_z \mathbf{u}'}$ is the viscous dissipation of energy, whereas $T_{E_k} = \overline{w'\mathbf{u}'_h} \cdot \overline{\mathbf{u}_h}$
 416 and $T_k = \overline{w' \frac{\mathbf{u}' \cdot \mathbf{u}'}{2}} + \frac{1}{\rho_0} \overline{w'p'}$ – $\nu \partial_z k$ redistribute energy on the vertical. Exchanges be-
 417 tween the resolved and subgrid reservoirs of kinetic energy are done via the mechanical
 418 shear term $\overline{w'\mathbf{u}'_h} \cdot \partial_z \overline{\mathbf{u}_h}$. To close the budgets, we provide in the following sections a bud-
 419 get for internal and potential energy.

420 **3.2 Internal and Potential energies**

421 For a generic fluid, the unaveraged specific internal energy can be written as

$$\mathcal{E}_i = \mathcal{h}(p, \phi) - \frac{p}{\rho} \quad (32)$$

422 where \mathcal{h} is the specific enthalpy and ϕ is any entropic variable describing components
 423 of the fluid. Under the Boussinesq approximation, internal energy is (Tailleux & Dubos,
 424 2023)

$$\mathcal{E}_i = \mathcal{h}(p_0, \phi) + (p_{\text{ref}} - p_0) \partial_p \mathcal{h}(p_0, \phi) - \frac{p_{\text{ref}}}{\rho_0} \quad (33)$$

425 where we recall that $p_{\text{ref}}(z) = -\rho_0 g z + p_0$, and the specific volume is by definition $1/\rho :=$
 426 $\partial_p \mathfrak{h}$. In particular, this implies that under the Boussinesq approximation $b(\phi) := -g(\rho(p_0, \phi) -$
 427 $\rho_0)/\rho(p_0, \phi)$ (e.g. sec. 3.4 of Eldred & Gay-Balmaz, 2021). The sum of unaveraged in-
 428 ternal and potential energies can then be written as

$$\mathcal{E}_i + E_p = z(g - b) + \mathfrak{h}(p_0, \phi) - \frac{p_0}{\rho_0} \quad (34)$$

429 which leads to the unaveraged budget (Young, 2010; Tailleux, 2012)

$$\partial_t(\mathcal{E}_i + E_p) + \nabla \cdot ([\mathfrak{h}(p_0, \phi) + gz] \mathbf{u}) = \epsilon_\nu - wb \quad (35)$$

430 Upon averaging and using the SCM assumptions, the budget of mean internal energy
 431 $E_i = \bar{\mathcal{E}}_i$ and potential energy reads

$$\partial_t(E_i + E_p) + \partial_z(\overline{\partial_\phi \mathfrak{h}_0} \overline{w' \phi'}) = \bar{\epsilon}_\nu - \partial_z(\overline{\phi} \overline{w' \partial_\phi \mathfrak{h}'_0} + \overline{\phi' w' \partial_\phi \mathfrak{h}'_0}) - \overline{w' b'} \quad (36)$$

432 where we introduced the notation $\mathfrak{h}_0(\phi) := \mathfrak{h}(p_0, \phi)$. Remark that if $\mathfrak{h}(p_0, \phi)$ is linear
 433 in ϕ , we have closed relations $\overline{\mathfrak{h}(p_0, \phi)} = \mathfrak{h}(p_0, \bar{\phi})$ and $\overline{b(\phi)} = b(\bar{\phi})$.

434 As a summary, the budgets of mean kinetic energy, turbulent kinetic energy and
 435 the sum of mean internal and potential energy are

$$\begin{cases} \partial_t E_k + \partial_z T_{E_k} & = \overline{w' \mathbf{u}'_h} \cdot \partial_z \bar{\mathbf{u}}_h \\ \partial_t k + \partial_z T_k & = -\overline{w' \mathbf{u}'_h} \cdot \partial_z \bar{\mathbf{u}}_h + \overline{w' b'} - \bar{\epsilon}_\nu \\ \partial_t(E_i + E_p) + \partial_z(\overline{\partial_\phi \mathfrak{h}_0} \overline{w' \phi'}) & = -\partial_z(\overline{\phi} \overline{w' \partial_\phi \mathfrak{h}'_0} + \overline{\phi' w' \partial_\phi \mathfrak{h}'_0}) - \overline{w' b'} + \bar{\epsilon}_\nu \end{cases} \quad (37)$$

436 where conversion of E_k into k occurs via mean shear, conversion of k into E_i occurs via
 437 viscous dissipation, and conversion of k into $E_i + E_p$ occurs via buoyancy fluxes.

438 In the following, we illustrate these budgets for dry atmosphere and seawater.

439 3.2.1 Dry atmosphere

440 The specific enthalpy for a dry atmosphere modeled as an ideal gas $p = \rho R_d T$ is

$$\mathfrak{h}(p, \theta) = c_p \left(\frac{p}{p_0} \right)^{R_d/c_p} \theta \quad (38)$$

441 which is linear in the potential temperature $\theta = T(p/p_0)^{-R_d/c_p}$. Using (33) the sum
 442 of mean internal and potential energy within the Boussinesq approximation is

$$E_i + E_p = \left(c_p - \frac{gz}{\theta_0} \right) \bar{\theta} + 2gz - \frac{p_0}{\rho_0} \quad (39)$$

443 and buoyancy is $b(\bar{\theta}) = g(\bar{\theta} - \theta_0)/\theta_0$. The budget of $E_i + E_p$ is

$$\partial_t(E_i + E_p) = \left(c_p - \frac{gz}{\theta_0} \right) \partial_t \bar{\theta} = \bar{\epsilon}_\nu - \partial_z \left(c_p \frac{\theta_0}{g} \overline{w' b'} \right) - \overline{w' b'} \quad (40)$$

444 where $\overline{w' b'} = \frac{g}{\theta_0} \overline{w' \theta'}$. As a summary, the budgets of mean kinetic energy, turbulent ki-
 445 netic energy and the sum of mean internal and potential energy for a *dry atmosphere* within
 446 the Boussinesq approximation are

$$\begin{cases} \partial_t E_k + \partial_z T_{E_k} & = \overline{w' \mathbf{u}'_h} \cdot \partial_z \bar{\mathbf{u}}_h \\ \partial_t k + \partial_z T_k & = -\overline{w' \mathbf{u}'_h} \cdot \partial_z \bar{\mathbf{u}}_h + \frac{g}{\theta_0} \overline{w' \theta'} - \bar{\epsilon}_\nu \\ \left(c_p - \frac{gz}{\theta_0} \right) \partial_t \bar{\theta} + -\partial_z \left(c_p \overline{w' \theta'} \right) & = -\frac{g}{\theta_0} \overline{w' \theta'} + \bar{\epsilon}_\nu \end{cases} \quad (41)$$

447 **3.2.2 Seawater with linearized equation of state**

448 For an ocean with a linearized equation of state, Boussinesq buoyancy is

$$b(\theta, S) = g\alpha(\theta - \theta_0) - g\beta(\theta - S_0) \quad (42)$$

449 and specific enthalpy is

$$h(p_0, \theta, S) = c_p\theta - gz(1 + \alpha(\theta - \theta_0) - \beta(\theta - S_0)) \quad (43)$$

450 Using (33), the budget of mean internal and potential energy is

$$\partial_t (c_p\bar{\theta} - z\bar{b}) = \bar{\epsilon}_\nu - \partial_z (c_p\overline{w'\theta'} - z\overline{w'b'}) - \overline{w'b'} \quad (44)$$

451 The budgets of mean kinetic energy, turbulent kinetic energy, and the sum of mean internal and potential energy for *seawater* with a linearized equation of state are

$$\begin{cases} \partial_t E_k + \partial_z T_{E_k} & = \overline{w'\mathbf{u}'_h} \cdot \partial_z \bar{\mathbf{u}}_h \\ \partial_t k + \partial_z T_k & = -\overline{w'\mathbf{u}'_h} \cdot \partial_z \bar{\mathbf{u}}_h + \overline{w'b'} - \bar{\epsilon}_\nu \\ \partial_t (c_p\bar{\theta} - z\bar{b}) + \partial_z T_{E_i+E_p} & = -\overline{w'b'} + \bar{\epsilon}_\nu \end{cases} \quad (45)$$

453 Using the salt budget $\partial_t \bar{S} = -\partial_z \overline{w'S'}$, we can split this last equation as

$$\partial_t \bar{\theta} = \frac{\bar{\epsilon}_\nu}{c_p - \alpha gz} - \partial_z \overline{w'\theta'} \quad (46)$$

$$\partial_t (-z\bar{b}) = -zg\alpha \frac{\bar{\epsilon}_\nu}{c_p - \alpha gz} + \partial_z (z\overline{w'b'}) - \overline{w'b'} \quad (47)$$

454 Since the energy increase due to viscous dissipation is negligible in the ocean, $-z\bar{b}$ is often used as a proxy for "potential" energy (e.g. McDougall, 2003; Olbers et al., 2012).
455 We nevertheless retain this dissipative heating in (46) to work with a properly closed energy budget in theoretical descriptions.
457

458 **4 Consistency of TKE equation with EDMF closures**

459 Based on the energy budgets described in the previous section, we provide a new parameterization of the TKE budget to obtain an energetically consistent model mimicking (37). Indeed, the following TKE equation is commonly used in TKE-based numerical models regardless of whether ED or EDMF closure is used,

$$\partial_t k + \partial_z (-K_k \partial_z k) = K_u \partial_z \bar{\mathbf{u}}_h \cdot \partial_z \bar{\mathbf{u}}_h - K_\phi \partial_z \bar{b} - \bar{\epsilon}_\nu \quad (48)$$

463 where k represents the turbulent kinetic of the whole grid cell, *i.e.* $1/2\overline{\mathbf{u}' \cdot \mathbf{u}'}$. In (48),
464 turbulent fluxes have been closed using ED. However, we argue that if an EDMF closure is used in the mean equations (for momentum, temperature, and salinity or humidity), the TKE equation should be modified by MF terms to ensure energetic consistency as shown below. Note that Tan et al. (2018) made a different choice by considering a budget for the *environmental* TKE, $k_e = 1/2\overline{\mathbf{u}'_e \cdot \mathbf{u}'_e}$.
468

469 **4.1 Shear and Buoyancy terms**

470 We have seen in (37) that sources of turbulent kinetic energy could arise from the mean kinetic energy via mean shear $-\overline{w'\mathbf{u}'_h} \cdot \partial_z \bar{\mathbf{u}}_h$, or from internal and potential energies via buoyancy production $\overline{w'b'}$.
472

473 When the EDMF approach is used to close fluxes in the diagnostic equations of $\bar{\mathbf{u}}_h$ and $\bar{\phi}$, then the same closures must be used in turbulent kinetic energy budget to ensure energetic consistency. As a consequence, the shear term must be closed as

$$-\overline{w'\mathbf{u}'_h} \cdot \partial_z \bar{\mathbf{u}}_h \Big|_{\text{EDMF}} = -[-K_u \partial_z \bar{\mathbf{u}}_h + a_p w_p (\mathbf{u}_{h,p} - \bar{\mathbf{u}}_h)] \cdot \partial_z \bar{\mathbf{u}}_h \quad (49)$$

476 In the case of *dry atmosphere*, the buoyancy production term is

$$\overline{w'b'}_{\text{EDMF}} = \frac{g}{\theta_0} [-K_\theta \partial_z \bar{\theta} + a_p w_p (\theta_p - \bar{\theta})] \quad (50)$$

477 whereas in the case of *seawater* with linearized equation of state and $K_\phi = K_\theta = K_S$,

$$\begin{aligned} \overline{w'b'}_{\text{EDMF}} &= g\alpha [-K_\theta \partial_z \bar{\theta} + a_p w_p (\theta_p - \bar{\theta})] - g\beta [-K_S \partial_z \bar{S} + a_p w_p (S_p - \bar{S})] \\ &= -K_\phi \partial_z \bar{b} + a_p w_p (b_p - \bar{b}) \end{aligned}$$

478 4.2 Fluxes of TKE

479 The redistribution terms of TKE are often little discussed in turbulence parameterization since they do not contribute directly to the vertically integrated energy budgets. However, they are of great importance in convective conditions where non-local transport dominates (Witek et al., 2011a). For instance, in the atmosphere, the TKE produced close to the surface due to destabilizing buoyancy fluxes is then transported by coherent plumes in the mixed layer. Taking into account MF transport of TKE is thus essential to achieve local energetic consistency, and model accurately TKE at any level z .

486 Turbulent fluxes of TKE arise from the contribution of a TKE transport term, a pressure redistribution term and a viscous flux,

$$T_k = \frac{1}{2} \overline{w' \mathbf{u}' \cdot \mathbf{u}'} + \frac{1}{\rho_0} \overline{w' p'} - \nu \partial_z k \quad (51)$$

488 For atmospheric and oceanic flow, the viscous flux is negligibly small and will be omitted. We will assume the pressure redistribution term to be small compared to the transport of TKE, as it is usually done in CBL schemes (e.g. Mellor, 1973). In numerical models, TKE transport is usually parameterized via K-diffusion, namely

$$\partial_z \left(\overline{w' \frac{\mathbf{u}' \cdot \mathbf{u}'}{2}} \right) \simeq -\partial_z (K_k \partial_z k) \quad (52)$$

492 However, within the framework exposed in section 2.1, we can apply the two-domain decomposition of the horizontal average to get the exact relation

$$\begin{aligned} \overline{w' \frac{\mathbf{u}' \cdot \mathbf{u}'}{2}} &= \sum_{i=e,p} a_i \underbrace{\frac{1}{2} \overline{\mathbf{u}'_i \cdot \mathbf{u}'_i w'_i}}_{\text{I}_i} + \underbrace{a_i (\mathbf{u}_i - \bar{\mathbf{u}}) \cdot \overline{\mathbf{u}'_i w'_i}}_{\text{II}_i} \\ &\quad + \underbrace{a_i (w_i - \bar{w}) \frac{1}{2} \overline{\mathbf{u}'_i \cdot \mathbf{u}'_i}}_{\text{III}_i} + \underbrace{a_i \frac{1}{2} (\mathbf{u}_i - \bar{\mathbf{u}})^2 (w_i - \bar{w})}_{\text{IV}_i} \end{aligned} \quad (53)$$

494 where: I_i is an intra-subdomain turbulent TKE transport; II_i is a transport of Reynolds stress by the coherent velocities; III_i is a transport of subdomain TKE by the coherent velocities (*i.e.* transport of TKE by mass-flux); IV_i is a transport of convective kinetic energy by coherent velocities. Based on LES simulations (see Sec. 5.3), we found that: (i) I_p can be neglected, consistently with the small area limit; (ii) II_e and II_p are almost compensating, thus the sum $\text{II}_e + \text{II}_p$ can be neglected. Using $a_p w_p = -a_e w_e$, we can conveniently reformulate the remaining terms:

$$\text{III}_e + \text{III}_p + \text{IV}_e + \text{IV}_p = a_p w_p \frac{1}{1 - a_p} \left(k_p + \frac{1}{2} \|\mathbf{u}_p - \bar{\mathbf{u}}\|^2 - k \right) \quad (54)$$

501 where we have used the following exact decomposition of TKE:

$$k = \frac{1}{2} a_e \|\mathbf{u}_e - \bar{\mathbf{u}}\|^2 + a_e k_e + \frac{1}{2} a_p \|\mathbf{u}_p - \bar{\mathbf{u}}\|^2 + a_p k_p \quad (55)$$

502 and $k_i := 1/2\overline{\mathbf{u}'_i \cdot \mathbf{u}'_i}$ ($i = e, p$). In EDMF closures, turbulence is assumed isotropic in
 503 the environment, thus we close $\frac{1}{2}\overline{\mathbf{u}'_e \cdot \mathbf{u}'_e w'_e}$ with K-diffusion, similar to the standard prac-
 504 tice for TKE-only schemes. Then assuming $\frac{1}{1-a_p} \simeq 1$ (i.e. the small area limit) we have

$$\overline{w' \frac{\mathbf{u}' \cdot \mathbf{u}'}{2}} \simeq \underbrace{-K_k \partial_z k}_{\text{ED}} + \underbrace{a_p w_p \left(k_p - k + \frac{1}{2} \|\mathbf{u}_p - \bar{\mathbf{u}}\|^2 \right)}_{\text{MF}} \quad (56)$$

505 It is interesting to note that we can recover existing formulations from the proposed clo-
 506 sure (56): if $a_p w_p = 0$ it boils down to the classical eddy-diffusivity closure; if $k_p = k$
 507 and $\mathbf{u}_{h,p} = \bar{\mathbf{u}}_h$ the term $1/2w_p^3$ proposed by Witek et al. (2011a) is recovered; if $\mathbf{u}_p =$
 508 $\bar{\mathbf{u}}$ then the formulation proposed by Han and Bretherton (2019) is recovered. However,
 509 we should mention that the latter authors treat TKE as a tracer to include the term $a_p w_p (k_p -$
 510 $k)$. This justification is incorrect because $w' \mathbf{u}' \cdot \mathbf{u}' / 2$ is not a second-order moment, but
 511 a third-order moment which requires a proper treatment as seen in (53).

512 Finally, one still needs to provide a value for k_p . Without any assumption, its prog-
 513 nostic equation reads (Tan et al., 2018, eq. (11))

$$\begin{aligned} \partial_t(a_p k_p) + \partial_z(a_p w_p k_p) &= -a_p \overline{w'_p \mathbf{u}'_{h,p}} \cdot \partial_z \mathbf{u}_{h,p} + a_p \overline{w'_p b'_p} \\ &+ E \left(k_e + \frac{1}{2} \|\mathbf{u}_e - \mathbf{u}_p\|^2 \right) - D k_p \\ &- \partial_z \left(a_p w'_p \frac{\mathbf{u}'_p \cdot \mathbf{u}'_p}{2} + a_p \mathbf{u}'_p \cdot \frac{1}{\rho_0} (\nabla p^\dagger)'_p \right) \\ &- a_p (\epsilon_\nu)_p \end{aligned}$$

514 As a first attempt, we propose to retain advection, entrainment, detrainment and dis-
 515 sipation terms, which lead to the simplified form of the previous equation:

$$\partial_z(a_p w_p k_p) = E \left(k_e + \frac{1}{2} \|\mathbf{u}_e - \mathbf{u}_p\|^2 \right) - D k_p - a_p (\epsilon_\nu)_p \quad (57)$$

$$= E \left(\frac{1}{1-a_p} k - \frac{a_p}{1-a_p} k_p + \frac{1}{1-a_p} \frac{1}{2} (\mathbf{u}_p - \bar{\mathbf{u}})^2 \right) - D k_p - a_p (\epsilon_\nu)_p \quad (58)$$

516 where we have used the identity $(\mathbf{u}_e - \mathbf{u}_p)^2 = \frac{1}{(1-a_p)^2} (\mathbf{u}_p - \bar{\mathbf{u}})^2$ and substituted k_e us-
 517 ing (55). Using area conservation, we get the advective form

$$a_p w_p \partial_z k_p = E \frac{1}{1-a_p} \left(k - k_p + \frac{1}{2} (\mathbf{u}_p - \bar{\mathbf{u}})^2 \right) - a_p (\epsilon_\nu)_p \quad (59)$$

518 Finally assuming $\frac{1}{1-a_p} \simeq 1$ (i.e. the small area limit) we have

$$a_p w_p \partial_z k_p = E \left(k - k_p + \frac{1}{2} (\mathbf{u}_p - \bar{\mathbf{u}})^2 \right) - a_p (\epsilon_\nu)_p \quad (60)$$

519 As a summary, the proposed closure of TKE transport is given by

$$\overline{w' \frac{\mathbf{u}' \cdot \mathbf{u}'}{2}} = -K_k \partial_z k + a_p w_p \left(k_p - k + \frac{1}{2} \|\mathbf{u}_p - \bar{\mathbf{u}}\|^2 \right) \quad (61)$$

$$a_p w_p \partial_z k_p = E \left(k - k_p + \frac{1}{2} (\mathbf{u}_p - \bar{\mathbf{u}})^2 \right) - a_p (\epsilon_\nu)_p \quad (62)$$

520 4.3 Viscous dissipation

521 The total viscous dissipation rate is often parameterized as $\bar{\epsilon}_\nu = \frac{c_\epsilon}{l_\epsilon} k^{3/2}$ in stan-
 522 dard ED schemes, we do the same for the plume viscous dissipation rate

$$(\epsilon_\nu)_p = \frac{c_\epsilon}{l_\epsilon} k_p^{3/2}$$

523 where $c_\epsilon = \sqrt{2}/2$ is a numerical constant and the dissipation length is $l_\epsilon = \sqrt{l_{\text{up}} l_{\text{dwn}}}$
 524 (e.g. Gaspar et al., 1990) with l_{up} and l_{dwn} defined in Appendix B.

525 **4.4 Boundary conditions**

526 In general, providing physically relevant boundary conditions for the TKE equa-
 527 tion is a complex question that we do not intend to answer in this study. However, once
 528 modelling choices are made, we can provide guidelines to utilize such boundary condi-
 529 tion consistently within an EDMF scheme.

530 **4.4.1 Generic constraint**

531 According to (61), the boundary condition should verify at $z = 0$

$$\overline{w' \frac{\mathbf{u}' \cdot \mathbf{u}'}{2}} = -K_k \partial_z k + a_p w_p \left(k_p - k + \frac{1}{2} \|\mathbf{u}_p - \bar{\mathbf{u}}\|^2 \right) \quad (63)$$

532 In general if plume variables are specified at $z = 0$, then (63) is again a Robin bound-
 533 ary condition for the TKE equation.

534 **4.4.2 Oceanic context**

535 In the ocean, we will assume the following boundary conditions,

$$\overline{w' \frac{\mathbf{u}' \cdot \mathbf{u}'}{2}} = 0, \quad k_p(0) = k(0)$$

536 along with $\mathbf{u}_p(0) = (\bar{u}(0), \bar{v}(0), w_p^0)$. In this case, (63) implies the following Neumann
 537 condition for TKE,

$$K_k \partial_z k(0) = \frac{1}{2} a_p^0 (w_p^0)^3 \quad (64)$$

538 Our formulation could handily include non-zero TKE flux at the surface, as proposed
 539 in the presence of wave-breaking (Craig & Banner, 1994; Mellor & Blumberg, 2004).

540 **4.4.3 Atmospheric context**

541 In atmospheric models, a value of TKE depending on friction and convective ve-
 542 locities is usually imposed at or near the surface, following field measurements of Wyngaard
 543 and Coté (1971). As long as the plume contribution to the surface TKE flux is imposed
 544 to be zero, the previous approach can be still used. If not, special care would have to be
 545 taken to enforce (63) and avoid spurious energy fluxes.

546 **4.5 EDMF-parameterized budgets**

547 Within the Boussinesq approximation, the budget of resolved kinetic energy, sub-
 548 grid kinetic energy, and resolved internal+potential energy for a *dry atmosphere* with
 549 EDMF closure is

$$\begin{cases} \partial_t E_k + \partial_z T_{E_k} & = -K_u (\partial_z \bar{\mathbf{u}}_h)^2 + a_p w_p (\mathbf{u}_{h,p} - \bar{\mathbf{u}}_h) \cdot \partial_z \bar{\mathbf{u}}_h \\ \partial_t k + \partial_z T_k & = \frac{g}{\theta_0} [-K_\theta \partial_z \bar{\theta} + a_p w_p (\theta_p - \bar{\theta})] + K_u (\partial_z \bar{\mathbf{u}}_h)^2 - a_p w_p (\mathbf{u}_{h,p} - \bar{\mathbf{u}}_h) \cdot \partial_z \bar{\mathbf{u}}_h - \bar{\epsilon}_\nu \\ \partial_t \left[\left(c_p - \frac{gz}{\theta_0} \right) \bar{\theta} \right] + \partial_z T_{E_i + E_p} & = -\frac{g}{\theta_0} [-K_\theta \partial_z \bar{\theta} + a_p w_p (\theta_p - \bar{\theta})] + \bar{\epsilon}_\nu \end{cases} \quad (65)$$

550 where the flux terms are

$$T_{E_k} = (-K_u \partial_z \bar{\mathbf{u}}_h + a_p w_p (\mathbf{u}_{h,p} - \bar{\mathbf{u}}_h)) \cdot \bar{\mathbf{u}}_h \quad (66)$$

$$T_k = -K_k \partial_z k + a_p w_p \left(k_p - k + \frac{1}{2} \|\mathbf{u}_p - \bar{\mathbf{u}}\|^2 \right) \quad (67)$$

$$T_{E_i + E_p} = -c_p K_\theta \partial_z \bar{\theta} + c_p a_p w_p (\theta_p - \bar{\theta}) \quad (68)$$

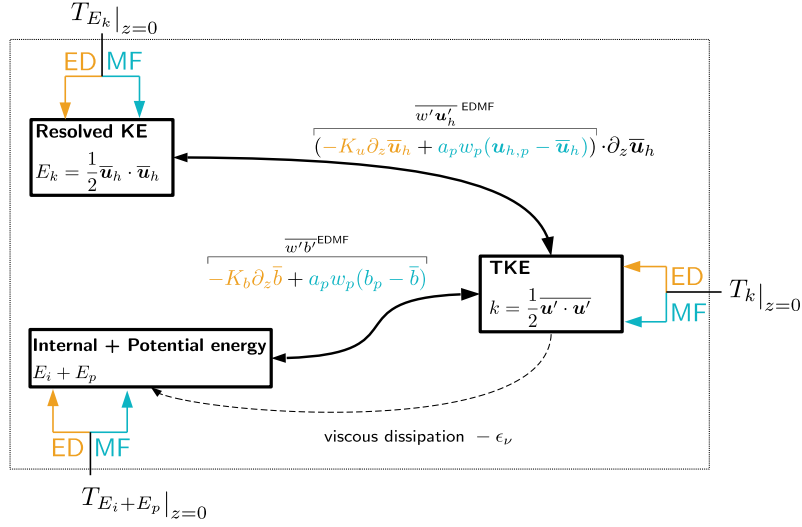


Figure 1: Schematic representation of bulk and boundary energy fluxes within EDMF closure (KE: kinetic energy, TKE: turbulent kinetic energy).

Equivalently, in the case of *seawater* with linearized equation of state

$$\begin{cases} \partial_t E_k + \partial_z T_{E_k} & = -K_u (\partial_z \bar{\mathbf{u}}_h)^2 + a_p w_p (\mathbf{u}_{h,p} - \bar{\mathbf{u}}_h) \cdot \partial_z \bar{\mathbf{u}}_h \\ \partial_t k + \partial_z T_k & = -K_\phi \partial_z \bar{b} + a_p w_p (b_p - \bar{b}) + K_u (\partial_z \bar{\mathbf{u}}_h)^2 - a_p w_p (\mathbf{u}_{h,p} - \bar{\mathbf{u}}_h) \cdot \partial_z \bar{\mathbf{u}}_h - \bar{\epsilon}_\nu \\ \partial_t (c_p \bar{\theta} - z\bar{b}) + \partial_z T_{E_i+E_p} & = -(-K_\phi \partial_z \bar{b} + a_p w_p (b_p - \bar{b})) + \bar{\epsilon}_\nu \end{cases} \quad (69)$$

where the flux of internal and potential energy is

$$T_{E_i+E_p} = -\partial_z (c_p (-K_\phi \partial_z \bar{\theta} + a_p w_p (\theta_p - \bar{\theta})) - z (-K_\phi \partial_z \bar{b} + a_p w_p (b_p - \bar{b}))) \quad (70)$$

and the conservative temperature equation is

$$\partial_t \bar{\theta} = \frac{\bar{\epsilon}_\nu}{c_p - \alpha g z} - \partial_z (-K_\phi \partial_z \bar{\theta} + a_p w_p (\theta_p - \bar{\theta}))$$

A summary of EDMF energy budgets is provided in Fig. 1 and in Tab. 2.

4.6 Vertically integrated energy budgets

In this section, we provide global energy budgets to highlight the role of mass-flux terms in bulk energy exchange as well as sinks/sources at boundaries. Let us introduce the vertical average $\langle X \rangle_z = 1/(\sigma_o^a H) \int_0^{\sigma_o^a H} X dz$, and the boundary operator $[X]_0^{\sigma_o^a H} = 1/(\sigma_o^a H)(X(z = \sigma_o^a H) - X(z = 0))$. Then for any advected field X with source term S_X , we have (see Appendix D for a detailed derivation):

$$\begin{aligned} \frac{1}{2} \partial_t \langle \bar{X}^2 \rangle_z &= \overbrace{-\langle K_X (\partial_z \bar{X})^2 \rangle_z}^{<0} - \overbrace{\left\langle \frac{E+D}{2} (X_p - \bar{X})^2 \right\rangle_z}^{<0} \\ &+ \langle \bar{X} \bar{S}_X \rangle_z + \langle a_p (S_X)_p (X_p - \bar{X}) \rangle_z \\ &- \left[\bar{X} \overline{w'X'} + a_p w_p \frac{(X_p - \bar{X})^2}{2} \right]_0^{\sigma_o^a H} \end{aligned}$$

561 Consequently, the entrainment and detrainment processes contribute on average to de-
 562 creasing the mean variance, similar to eddy-diffusivity terms. Although not sufficient in
 563 the context of nonlinear equations, monotonically decreasing variance is usually a nec-
 564 essary property to ensure analytical well-posedness of transport partial differential equa-
 565 tions (e.g. Evans, 2010). Interestingly, the last term of the budget implies that a non-
 566 zero MF flux at the boundary leads to an additional sink of resolved variance (which is
 567 exactly compensated by an equal and opposite boundary source for $\overline{X'^2}$).

568 We use (71) to get the vertically integrated mean kinetic energy budget,

$$\begin{aligned} \partial_t \langle E_k \rangle_z &= - \langle K_u (\partial_z \overline{\mathbf{u}}_h)^2 \rangle_z - \left\langle \frac{E + D}{2(1 - C_u)} (\mathbf{u}_{h,p} - \overline{\mathbf{u}}_h)^2 \right\rangle_z \\ &\quad - \left[\overline{\mathbf{u}}_h \cdot \overline{w' \mathbf{u}'_h} \right]_0^{\sigma_o^a H} - \left[\frac{a_p w_p}{2(1 - C_u)} (\mathbf{u}_{h,p} - \overline{\mathbf{u}}_h)^2 \right]_0^{\sigma_o^a H} \end{aligned}$$

569 and the vertically integrated TKE budget

$$\begin{aligned} \partial_t \langle k \rangle_z &= - \langle K_\phi \partial_z \overline{b} \rangle_z + \langle a_p w_p (b_p - \overline{b}) \rangle_z \\ &\quad + \langle K_u (\partial_z \overline{\mathbf{u}}_h)^2 \rangle_z + \left\langle \frac{E + D}{2(1 - C_u)} (\mathbf{u}_{h,p} - \overline{\mathbf{u}}_h)^2 \right\rangle_z \\ &\quad - \langle \overline{\epsilon}_\nu \rangle_z - [T_k]_0^{\sigma_o^a H} + \left[\frac{a_p w_p}{2(1 - C_u)} (\mathbf{u}_{h,p} - \overline{\mathbf{u}}_h)^2 \right]_0^{\sigma_o^a H} \end{aligned}$$

570 It is interesting to note that the parameterization of the plume horizontal pressure gra-
 571 dient introduced in 2.3.2 and characterized by the parameter C_u induces a hyperbolic
 572 enhancement of the transfer from E_k to k due to entrainment/detrainment processes.
 573 Additionally, the vertically integrated potential energy and resolved internal energy bud-
 574 get reads

$$\partial_t \langle E_i + E_p \rangle_z = \langle K_\phi \partial_z \overline{b} \rangle_z - \langle a_p w_p (b_p - \overline{b}) \rangle_z + \langle \overline{\epsilon}_\nu \rangle_z - [T_{E_i + E_p}]_0^{\sigma_o^a H} \quad (71)$$

575 To illustrate potential biases, let us examine the atmospheric surface flux at $z = 0$

$$T_{E_i + E_p}(0) = -c_p K_\theta \partial_z \overline{\theta}(0) + c_p a_p(0) w_p(0) (\theta_p(0) - \overline{\theta}(0))$$

576 and assume that the boundary condition is $-K_\theta \partial_z \overline{\theta}(0) = \overline{w' \theta'}(0)$ (for instance using
 577 MOST), along with a plume initialization of the form (28). Then we would have

$$T_{E_i + E_p}(0) = c_p \overline{w' \theta'}(0) + c_p \overline{w' \theta'}(0) \frac{a_p(0) w_p(0) \beta}{\sqrt{k(0)}}$$

578 where the second term leads to an unphysical source of energy for $a_p(0) w_p(0) \neq 0$. This
 579 bias is due to an inconsistent partitioning of the physical boundary flux $c_p \overline{w' \theta'}(0)$ into ED
 580 and MF fluxes.

581 5 Evaluation of the EDMF-Energy scheme using a single column model

582 In this section, we numerically evaluate the proposed EDMF formulation on three
 583 cases of oceanic deep convection. The first two cases are performed in an idealized set-
 584 ting and compared to Large Eddy Simulation (LES) data, whereas the last case is ini-
 585 tialized and forced with realistic data and compared to *in situ* measurements at the LION
 586 buoy in the Mediterranean Sea.

587 5.1 Description of idealized cases

588 The two idealized cases considered are reminiscent of typical deep convective condi-
 589 tions in the ocean (e.g. Marshall & Schott, 1999), where convection into a initially rest-
 590 ing ocean of constant stratification $\Delta\theta = 1 \text{ K}/1000 \text{ m}$ (corresponding $N_0^2 = 1.962 \times$

$\partial_t E_k + \partial_z T_{E_k}$	$= -K_u(\partial_z \bar{\mathbf{u}}_h)^2 + a_p w_p (\mathbf{u}_{h,p} - \bar{\mathbf{u}}_h) \cdot \partial_z \bar{\mathbf{u}}_h$	Resolved kinetic energy budget
$\partial_t (E_i + E_p) + \partial_z T_{E_i + E_p}$	$= -(-K_\phi \partial_z \bar{b} + a_p w_p (b_p - \bar{b})) + \bar{\epsilon}_\nu$	Internal and potential energy budget
$\partial_t k - \partial_z (K_k \partial_z k)$	$= K_u(\partial_z \bar{\mathbf{u}}_h)^2 - K_\phi \partial_z \bar{b}$	ED related TKE production terms
	$-a_p w_p (\mathbf{u}_{h,p} - \bar{\mathbf{u}}_h) \cdot \partial_z \bar{\mathbf{u}}_h + a_p w_p (b_p - \bar{b})$	MF related TKE production terms
	$-\partial_z \left(a_p w_p \left[k_p - k + \frac{1}{2} \ \mathbf{u}_p - \mathbf{u}\ ^2 \right] \right)$	MF related TKE transport term
	$-\bar{\epsilon}_\nu$	TKE dissipation
$a_p w_p \partial_z k_p$	$= E \left(k - k_p + \frac{1}{2} \ \mathbf{u}_p - \mathbf{u}\ ^2 \right) - a_p (\epsilon_\nu)_p$	Plume related TKE
K_k	$= c_k l_m \sqrt{k}$	TKE eddy-diffusivity

Table 2: Complementary equations to those presented in Tab. 1, derived from energy consistency constraints in Sec. 4.

591 10^{-6} s^{-2}) is triggered by a surface cooling of $Q_0 = -500 \text{ W m}^{-2}$ (corresponding to a
 592 surface buoyancy loss of $B_0 = -2.456 \times 10^{-7} \text{ m}^2 \text{ s}^{-3}$). In both cases, salinity is kept
 593 uniform at $S = 32.6$ psu. The first case (FC500) consists of free convection, where no
 594 wind stress is applied. In the second idealized case (W005_C500) a uniform wind stress
 595 along the meridional direction, of magnitude $(u_*^a)^2 = 0.05 \text{ m}^2 \text{ s}^{-2}$, is applied. A sum-
 596 mmary of the parameters for each case can be found in table 3. To characterize wind-shear
 597 effects, we introduce the Froude number (Haghsheenas & Mellado, 2019)

$$Fr_* = \frac{u_*^o}{N_0 L_0} \quad (72)$$

598 where the length scale $L_0 = (B_0/N_0^3)^{1/2}$ can be interpreted as an Ozmidov scale $(\bar{\epsilon}_\nu/N^3)^{1/2}$
 599 (Garcia & Mellado, 2014) which is a measure of the smallest eddy size affected by a back-
 600 ground stratification N_0^2 in a turbulent field characterized by a viscous dissipation rate
 601 ϵ_ν . After $t_f = 72$ h of simulation leading to a mixed layer depth h (defined as the depth
 602 at which the buoyancy flux is minimum) of several hundred meters, various non-dimensional
 603 numbers can be used to characterize the flow. Their values can be found in Tab. 4. The
 604 ratio of the mixed layer depth to the Obukhov length (Obukhov (1971) and Zheng et
 605 al. (2021) in the oceanic context) h/L_{Ob} , where

$$L_{Ob} = \frac{(u_*^o)^3}{-B_0}$$

606 is an estimate of the depth at which the production of TKE by turbulent shear is of the
 607 same order of magnitude as the production of TKE by buoyancy fluxes. Noting $w_* =$
 608 $(-B_0 h)^{1/3}$ the convective velocity scale (Deardorff, 1970), we get

$$\frac{h}{L_{Ob}} = \left(\frac{w_*}{u_*} \right)^3 \quad (73)$$

609 We also recall that the oceanic friction velocity u_*^o satisfies $\rho_o (u_*^o)^2 = \rho_a (u_*^a)^2$. The Richard-
 610 son number at the mixed layer base,

$$Ri_h = \frac{N_0^2}{\left(\frac{u_*^o}{h} \right)^2}$$

611 measures the destabilization by surface shear stresses of a stably stratified water column.
 612 At $t_f = 72$ h, the case W005_C500 can be described by $h/L_{Ob} \simeq 5.7$ and $Ri_h \simeq 310$,

Table 3: Idealized cases parameters

Case	Q_0 (W m^{-2})	$(u_*^a)^2$ ($\text{m}^2 \text{s}^{-2}$)	N_0^2 (s^{-2})	t_f (h)	Fr_*
FC500	-500	0	1.962×10^{-6}	72	0
W005_C500	-500	0.05	1.962×10^{-6}	72	0.56

Table 4: Idealized cases non-dimensional parameters after 72 h of simulation

Case	h/L_{Ob}	Ri_h	Ri_*
FC500	∞	∞	97
W05_C500	5.7	310	97

613 which corresponds to a regime of strong deepening of the MLD according to Legay et
 614 al. (2023). Finally, for free convection cases (no wind) a convective Richardson number
 615 can be built as

$$Ri_* = \frac{N_0^2}{(w_*/h)^2} = \frac{N_0^2 h^{4/3}}{(-B_0)^{2/3}} = Ri_h \left(\frac{L_{Ob}}{h} \right)^{2/3}$$

616 It can be interpreted as follows. The time evolution of the mixed layer depth can be ac-
 617 curately described by the scaling (Turner, 1979; Van Roekel et al., 2018)

$$h \propto h_{\text{enc}} \quad (74)$$

618 where the *encroachment* depth is $h_{\text{enc}}(t) := \sqrt{2 \frac{(-B_0)}{N_0^2} t}$. Then the ratio of the entrain-
 619 ment velocity $w_e = \frac{d}{dt}h$ to the convective velocity $w_* = (-B_0 h)^{1/3}$ reads

$$\frac{w_e}{w_*} \propto Ri_*^{-1} \quad (75)$$

620 5.2 LES model description and conditional sampling

621 The LES data have been generated by the Ocean-LES version of the non-hydrostatic
 622 model Méso-NH (Lac et al., 2018). It is solving an anelastic Lipps-Hemler system adapted
 623 to the ocean, along with a linearized equation of state. The model uses a second-order
 624 Runge-Kutta time stepping and spatial discretization of advection operators is performed
 625 with a fourth-order centered scheme. Explicit subgrid scale closures are computed via
 626 a 3-D turbulence scheme based on a prognostic equation of the subgrid turbulent kinetic
 627 energy using a mixing-length scale, computed from the volume of a grid cell (Cuxart et
 628 al., 2000). The domain size is 1000 m on the vertical and $7.5 \text{ km} \times 7.5 \text{ km}$ on the horizon-
 629 tal, where doubly periodic conditions are applied. A resolution of 10 m on the vertical
 630 and 15 m on the horizontal is used. Each configuration is run for 72 h with a time-step
 631 of 10 s. To assess the quality of the simulations, we checked that the subgrid TKE was
 632 never exceeding 20% of the TKE explicitly resolved by the LES (Pope, 2004). Via anal-
 633 ysis of the total TKE budget, we checked that a quasi-steady regime is reached after a
 634 few hours of simulation (e.g. Garcia & Mellado, 2014). Moreover, at the end of the sim-
 635 ulations, the typical size of coherent structures, which can be quantified by the horizon-
 636 tal integral length scale in the bulk of the mixed layer, is of the order $O(500 \text{ m}) \ll 7.5 \text{ km}$.
 637 This suggests that the horizontal domain is large enough to provide a satisfactory sam-
 638 pling of turbulent structures.

639 To identify plumes, we use a velocity-based conditional sampling adapted from Pergaud
 640 et al. (2009), namely the plume area is defined as

$$A_p(z, t) = \left\{ (x, y, z, t) \text{ such that } \bar{w}(z, t) - w(x, y, z, t) > m \times \max(\sqrt{w^{2'}}(z, t), \sigma_{\min}(z, t)) \right\} \quad (76)$$

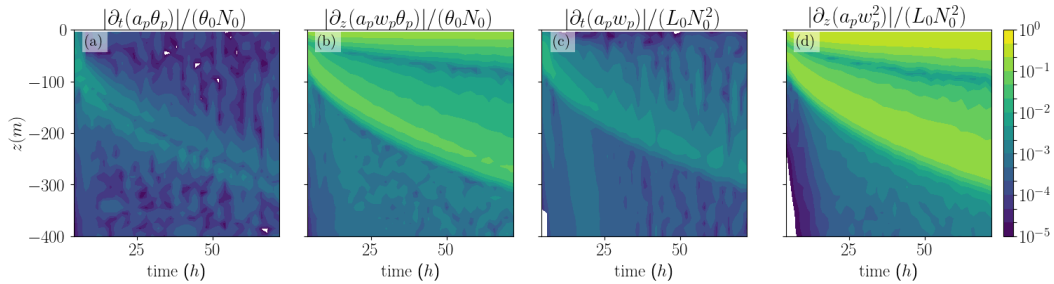


Figure 2: Temporal evolution of the normalized plume tendency $\partial_t(a_p X_p)$ and plume advection $\partial_z(a_p w_p X_p)$ terms, for the case FC500.

641 where the minimum standard deviation is chosen as $\sigma_{\min}(z, t) = 0.05/(-z) \int_z^0 \sqrt{w'^2}(z', t) dz'$.
 642 We checked that the qualitative results were not sensitive to m , and used $m = 1$ for
 643 the remainder. We do not use the tracer-based sampling of Couvreux et al. (2010) since
 644 it is valid only for small variations of the mixed layer depth. We neither utilize the "strong
 645 updraft" sampling of (Siebesma et al., 2007) since it assumes that a_p is a given constant.
 646 However, we checked that similar conclusions could be drawn from such samplings (not
 647 shown).

648 5.3 Validity of the steady plume hypothesis and small area limit

649 In this section, we directly evaluate the validity of the assumptions made in Sec.
 650 2.2 during the derivation of the proposed EDMF scheme against LES data. Fig. 2 shows
 651 that the plume temporal tendency terms are $O(10^{-2})$ smaller than plume advective terms
 652 which is consistent with the scaling in $1/(N_0 t)$ derived in 2.2.3. This justifies the use of
 653 the steady plume hypothesis. Fig. 3 shows vertical profiles of temperature, vertical ve-
 654 locity, plume fractional area, and temperature flux for the FC500 case. The small area
 655 assumption is roughly validated, with values of $a_p(z)$ between 10% and 20% of the total
 656 area, as exposed in previous studies (e.g. Couvreux et al., 2010). This justifies ques-
 657 tioning the relevance of this assumption and considering the system described in Appendix
 658 A. The convective velocity w_* is found to be a good estimate of the plume vertical ve-
 659 locity w_p . The contribution of the mass-flux term $a_p w_p (\theta_p - \bar{\theta})$ to the total tempera-
 660 ture flux is increasing with depth, until reaching a quasi-perfect match in the entrain-
 661 ment layer. The rough validity of assumption $a_p w_p (\theta_p - \bar{\theta}) \gg a_p \overline{w'_p \theta'_p}, a_e w_e (\theta_e - \bar{\theta})$ is
 662 consistent with the rough validity of $a_p \ll 1$. The plume/environment decomposition
 663 of the vertical transport of TKE $1/2 \overline{w' \mathbf{u}' \cdot \mathbf{u}'}$ is presented in Fig. 3(e). The dominant
 664 terms exposed in (54) explain well the total flux.

665 All the previous findings are also verified for the W005_C500 case (not shown).

666 5.4 SCM evaluation

667 In this section, we evaluate three different configurations of the SCM against LES
 668 data. First, a setup where only an eddy-diffusivity closure is used (referred as "ED"), and
 669 where the TKE equation (48) does not contain MF terms, which is equivalent to setting
 670 $a_p w_p = 0$. Second, an EDMF scheme in which an ED closure of the TKE equation (48)
 671 is used (referred as "EDMF"). This configuration is not energetically consistent as ex-
 672 plained in Sec. 4. It would be the result of a naive independent coupling of TKE and
 673 MF schemes. Finally, the third configuration consists of the previously detailed EDMF
 674 scheme in which the TKE equation is modified as in (69) to include the contribution of
 675 MF terms to energy transfers (referred to as "EDMF-Energy"). Since the small area hy-

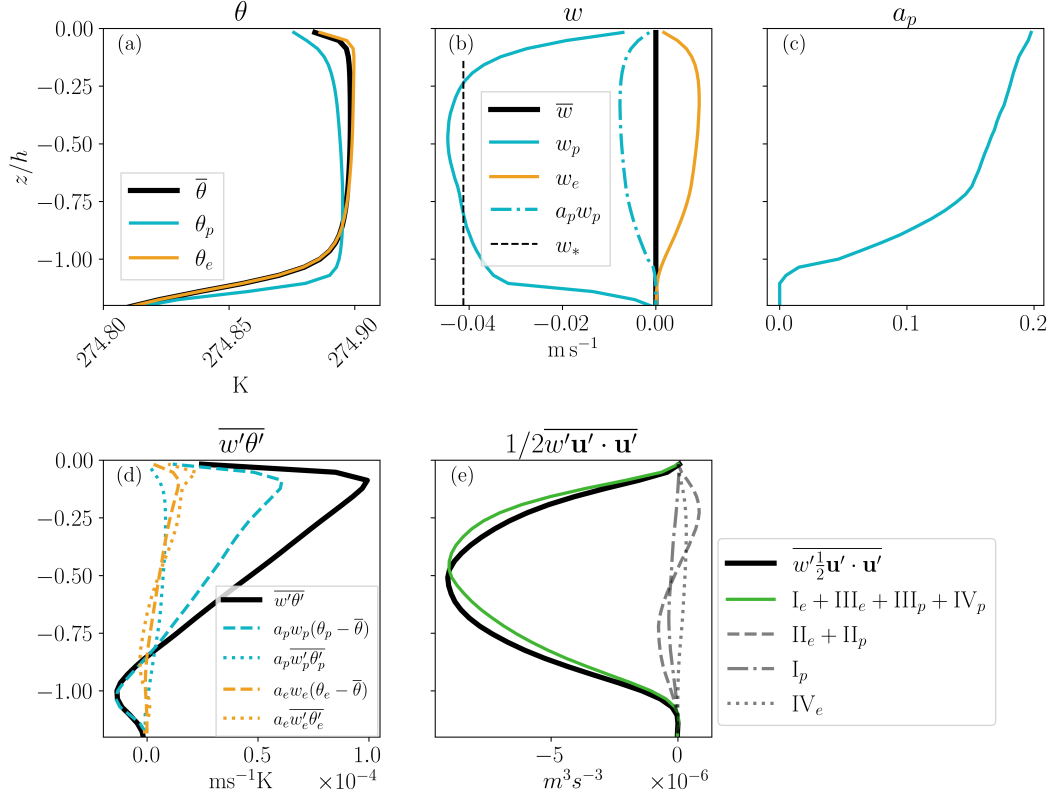


Figure 3: LES vertical profiles of (a) temperature, (b) vertical velocities, (c) plume fractional area, (d) temperature flux and (e) TKE flux for the FC500 case after 72 h of simulation. For each field, the black lines represent an horizontal average over the whole grid cell, the blue lines represent an average over the plume area and the orange lines represent an average over the environment area. In panel (b) the blue dotted line represents $a_p w_p$, and the gray dashed line represents the value of the free convective velocity scale w_* . In panel (d), total flux is in black, plume fluxes in blue (MF is dashed and subplume is dotted), and environment fluxes in orange (same linestyles). In panel (e) are represented the total flux (black) and the contributions from the combined terms $I_e + III_e + III_p + IV_p$ (blue), $II_e + II_p$ (dashed gray), I_p (dash-dotted gray) and III_p (dotted gray) (see 4.2 for details).

676 pothesis is approximately valid in LES, we also tested the relaxed version of table 1. How-
 677 ever, we could not identify significant impacts on such an idealized setup (not shown).
 678 For the three configurations, the constants c_m, c_ϵ, c_k used in the ED terms are the same
 679 as the constants used in the TKE equation of the LES model. The parameters used for
 680 the plume equations closures have been chosen as $\beta_1 = 0.99, \beta_2 = 1.99, a = 1.0, b =$
 681 $1.25, b' = 0.003 \text{ m}^{-1}, C_u = 0.5, a_p^0 = 0.2, \delta_0 = 0.005 \text{ m}^{-1}$. A careful tuning and uncer-
 682 tainty quantification of the parameters, using for instance statistical method (e.g. Souza
 683 et al., 2020; Couvreur et al., 2021), is left for future studies.

684 The examination of mean temperature and flux of temperature profiles shows that
 685 ED fails to reproduce the so-called vertical entrainment zone (e.g. Garcia & Mellado,
 686 2014), in which penetrative convection generates negative temperature flux and sharp-
 687 ens the temperature gradients at the base of the mixed layer. The lack of penetrative
 688 convection is known to reduce the deepening rate (e.g. chap. 6, Garratt, 1994a), thus
 689 producing an important bias of a hundred meters regarding the mixed layer depth com-
 690 pared to LES. On the other hand, EDMF and EDMF-energy equally perform in repre-
 691 senting these profiles. The absence of a noticeable effect of the energetic consistency on
 692 the temperature mean and flux profiles is a consequence of the small value of the ED fluxes
 693 (dashed lines) in the mixed layer. When considering the TKE profile, ED can model the
 694 correct order of magnitude, however, the TKE does not penetrate enough. EDMF fails
 695 to reproduce TKE due to energetic inconsistency. Indeed, looking at temperature and
 696 velocity fluxes allows us to infer that the losses of resolved energy due to buoyancy and
 697 shear are dominated by the MF contributions. However, such contributions are not in-
 698 cluded as sources of TKE for the EDMF scheme, leading to the very low levels of TKE
 699 observed in the simulation. EDMF-energy can reproduce accurate profiles of TKE. The
 700 main discrepancies arise close to the surface and at the base of the mixed layer. Neither
 701 ED nor EDMF can reproduce the vertical transport of TKE, whereas EDMF-energy re-
 702 produces well the profile. Similar conclusions are drawn from the WC005_C500 case (see
 703 Fig. 5).

704 In Fig. 6, we represent the vertically integrated energy budget of the SCM for the
 705 case W005_C500 (FC500 is similar), namely the quantity

$$\int_{-H}^0 \partial_t (E_k + k + E_i + E_p) dz + [T_{E_k} + T_k + T_{E_i+E_p}]_{-H}^0 \quad (77)$$

706 As expected, EDMF-energy conserves energy, whereas EDMF does not. The energy loss
 707 due to inconsistent energetics is equal to

$$\int_{-H}^0 (-a_p w_p (b_p - \bar{b}) + a_p w_p (\mathbf{u}_{h,p} - \bar{\mathbf{u}}_h) \cdot \partial_z \bar{\mathbf{u}}_h) dz \quad (78)$$

708 and scales with $B_0 h$.

709 5.5 Realistic case: Hymex/ASICS-MED campaign

710 We now move to more realistic situations corresponding to a sequence of strong con-
 711 vective events which were documented in the Northwestern Mediterranean during the
 712 winter 2013 of the HyMeX/ASICS-MED experiment at the LION buoy. This experiment
 713 was also carried out by Giordani et al. (2020) and we use a similar setup here (similar
 714 vertical grid as well as similar initial and surface boundary conditions). The experiments
 715 are performed with a SCM similar to (6) and (7) but including additional Coriolis and
 716 solar penetration (using a standard Jerlov law) terms. We consider conservative tem-
 717 perature and salinity as entropic variables which are related to buoyancy via a nonlin-
 718 ear equation of state. We also include penalization terms in the SCM to account for the
 719 effect of the bottom (which is at a depth of 2400 m at the LION buoy). Thanks to the
 720 penalization term a no-slip boundary condition is imposed at the bottom and a no-gradient
 721 condition is imposed for tracers. The vertical grid resolution ranges from 1 m near the

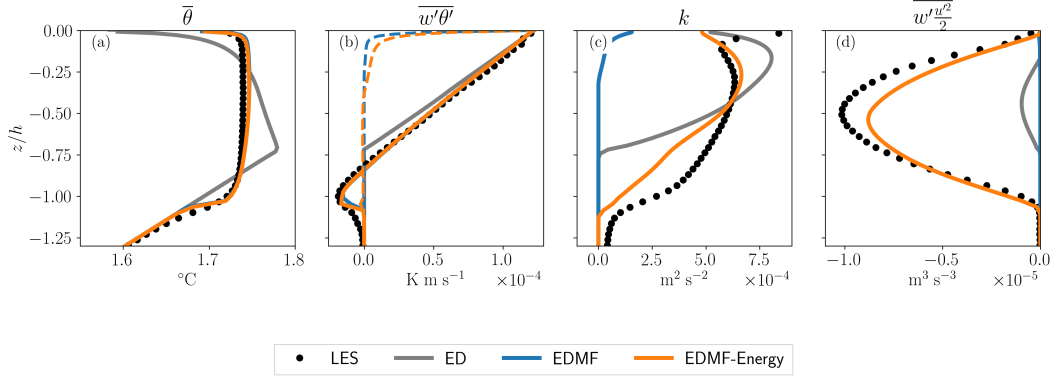


Figure 4: Vertical profiles of (a) temperature, (b) temperature flux, (c) turbulent kinetic energy and (d) turbulent transport of TKE for the FC500 case after 72h of simulation. LES data (black dots), ED-only scheme (grey line), standard EDMF scheme (blue line) and energetically consistent EDMF (orange line) are represented, along with the ED contribution to the temperature fluxes (dashed lines).

722 surface to 150 m near the bottom located at $z = -2400$ m. Parameters of the TKE
 723 scheme are set to the standard NEMO values, $\mathbf{c} = (c_m, c_e, c_k) = (0.1, \frac{\sqrt{2}}{2}, 0.1)$.

724 A series of 30-days numerical simulations were carried out starting from January
 725 15, 2013. The surface boundary conditions are shown in Fig. 7. In particular, very strong
 726 cooling events occurred during the period of interest. Two simulations were made sys-
 727 tematically with an eddy-diffusivity term activated. A first simulation was done with En-
 728 hanced Vertical Diffusion (referred to as ED+EVD) which is the standard practice for
 729 climate simulations using NEMO, a second one using a mass flux scheme on tracers, dy-
 730 namics, and with the additional terms for energetic consistency in the TKE equation (re-
 731 ferred to as EDMF-energy). To get a more concrete idea of the improvements brought
 732 about by the mass flux scheme over the usual practice for NEMO applications (ED+EVD),
 733 we show in Fig. 7 (bottom panel) the temporal evolution of the mixed layer depth h_{mixl}
 734 computed from mooring data and single-column numerical simulations. h_{mixl} is defined
 735 as the depth where the following criterion is met

$$\int_{h_{\text{mixl}}}^{z_{\text{ref}}} \partial_z b_{\text{eos}}(\theta, S = 38.5 \text{ psu}) dz = \frac{g}{\rho_0} \rho_c$$

736 with $z_{\text{ref}} = 300$ m and $\rho_c = 0.01 \text{ kg m}^{-3}$. We had to consider a constant salinity in
 737 the buoyancy calculation because the salinity data from the LION buoy are noisy in the
 738 vertical and did not allow for a robust diagnostics. The bottom panel in Fig. 7 illustrates
 739 the fact that the penetration depth of convective plumes is significantly better represented
 740 by the EDMF-Energy scheme than by the ED+EVD approach. Moreover, a direct compar-
 741 ison with temperature and salinity from mooring data is shown in Fig. 8 at differ-
 742 ent times. In particular several phases can be identified during the experiment (e.g. Cop-
 743 pola et al., 2017; Waldman et al., 2017): (i) in the period 15-25 January 2013 winter
 744 convection starts to deepen the mixed layer down to around -800 m to the point of erod-
 745 ing the Levantine intermediate waters. (ii) in the period 26-29 January 2013 the mixed
 746 layer keeps thickening to the depth of the western Mediterranean deep water (≈ -1250 m)
 747 (iii) in the period 4-9 February 2013 a new intense convective event associated with a
 748 strong Mistral event contributes to deepen the mixed layer down to the bottom (reached
 749 in 9 February). This is followed by a restratification phase involving horizontal processes
 750 that cannot be represented in our SCM formalism which explains why we do not ana-
 751 lyze solutions beyond February 9.

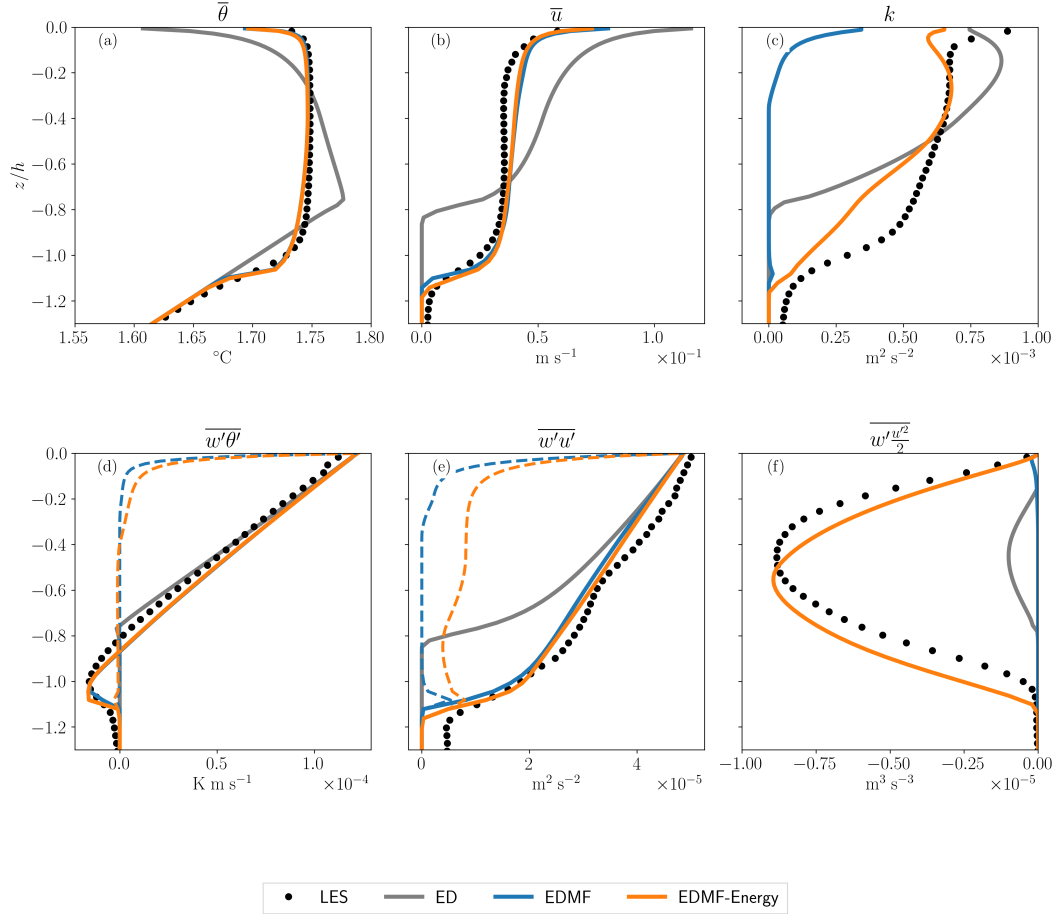


Figure 5: Vertical profiles of (a) mean temperature, (b) mean zonal current, (c) turbulent kinetic energy, (d) temperature flux, (e) zonal momentum flux, (d) turbulent transport of TKE for the FC500 case after 72h of simulation. LES data (black dots), ED-only scheme (grey line), standard EDMF scheme (blue line) and energetically-consistent EDMF (orange line) are represented, along with the ED contribution to the temperature and momentum fluxes (dashed lines).

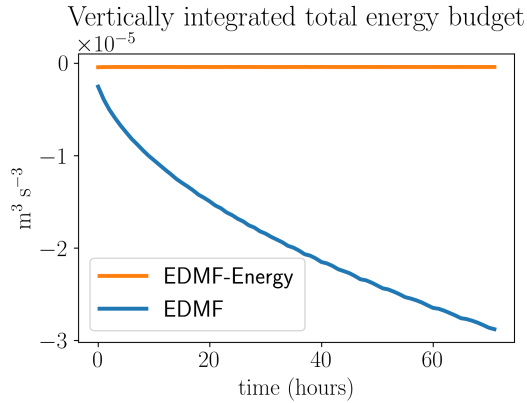


Figure 6: Time series of the vertically integrated energy budget (77) for the case W005_C500 (see text for details).

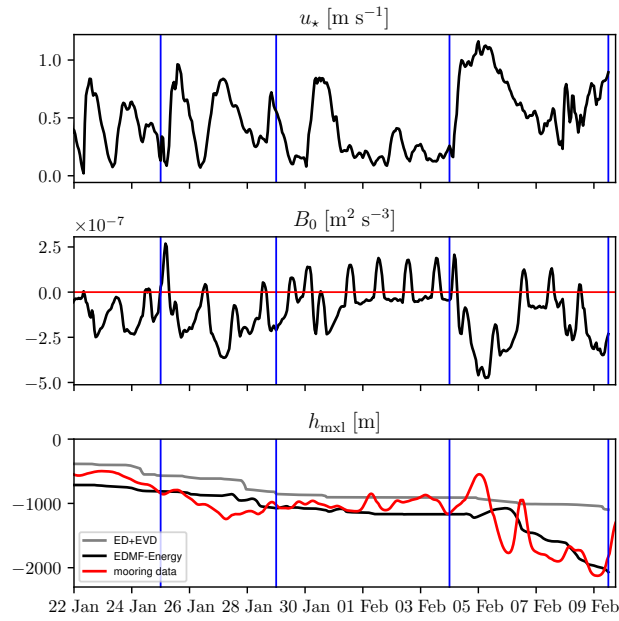


Figure 7: Time series of the friction velocity u_* (m s^{-1} , top panel) and surface buoyancy flux B_0 ($\text{m}^2 \text{s}^{-3}$, middle panel) computed from atmospheric forcings. Time series of mixed layer depth h_{mixl} (m, bottom panel) obtained from observations at the LION buoy (red line) and from single column numerical experiments using ED+EVD (solid gray line) and EDMF-Energy (solid black line). The vertical blue lines correspond to the dates at which the vertical temperature and salinity profiles derived from observations and numerical simulations are compared in Fig. 8.

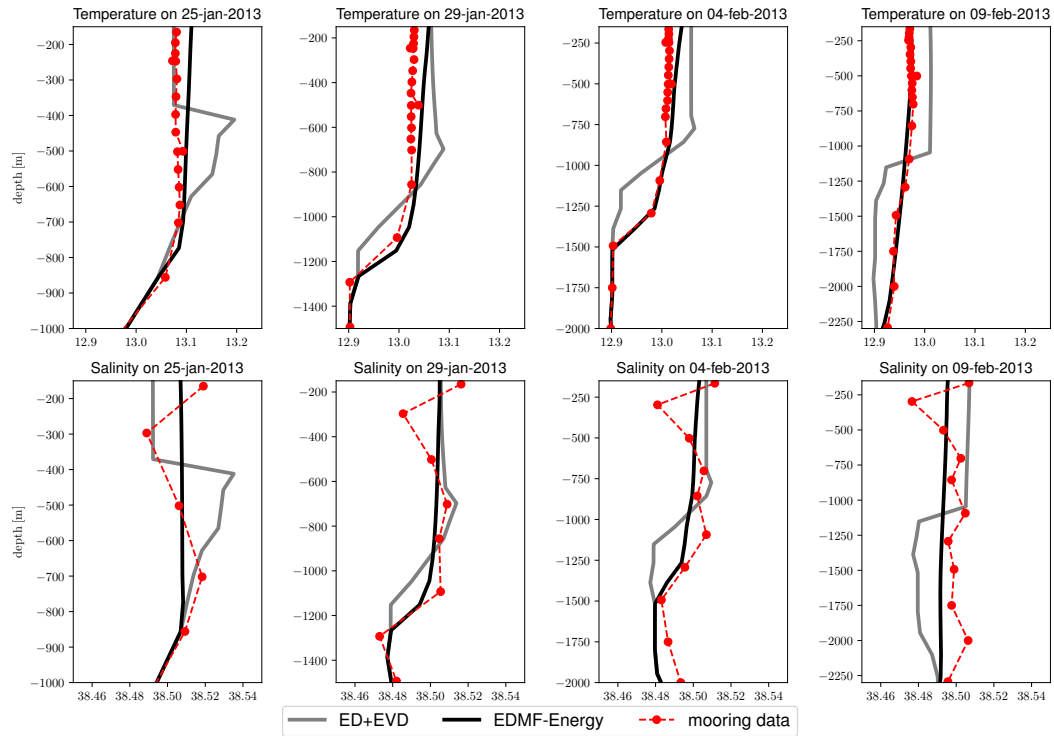


Figure 8: Temperature ($^{\circ}\text{C}$, top panels) and salinity (psu, bottom panels) profiles obtained from single column experiments at the location of the LION buoy using an eddy-diffusivity closure with enhanced vertical diffusion (ED-EVD, solid gray lines) and energetically-consistent EDMF (EDMF-Energy, solid black lines). Results from numerical experiments are compared to observations from the LION buoy (dashed red lines) for 4 dates represented on the Fig. 7 by vertical blue lines.

6 Discussion and conclusion

In this work, we have presented the theoretical derivation of an EDMF scheme with special attention paid to energetic aspects in a simple thermodynamic setting, for both dry atmosphere and seawater with linearized equation of state. During the derivation, we systematically reviewed the approximations used and provided both *a priori* scaling estimations, and direct evaluations of their validity on two idealized LES of oceanic convection. Closed energetics at the SCM level is a necessary step to obtain energetically consistent 3D models and thus reduce spurious energy biases. Theoretical horizontally averaged energy budgets are guiding the derivation of consistent energy budgets for SCM with EDMF closure. In particular, we have exposed the necessary modification of the standard TKE equation that incorporates EDMF terms to obtain closed energy budgets. Besides taking into account MF terms in shear and buoyancy terms, we propose an MF parameterization of TKE transport based on LES diagnostics. It generalizes previous formulations and implies the consideration of a subplume TKE (Han & Bretherton, 2019). We also show that boundary conditions on both mean and plume variables should be consistent with the EDMF decomposition to avoid spurious energy fluxes at the boundary and subsequent inconsistent energetics. We evaluate the performance of the proposed energetically consistent EDMF scheme in the context of idealized oceanic convection. When compared with LES of idealized oceanic convection, our scheme can reproduce mean fields and vertical fluxes of temperature and momentum as well as a non-energetically closed EDMF scheme. However energetic consistency is key to obtaining realistic TKE and turbulent transport of TKE profiles. To further illustrate that the MF concept is a credible alternative to the traditional approaches used in the oceanic context (using an enhanced vertical diffusion or a counter gradient term *à la* KPP (Large et al., 1994)) the proposed scheme is validated in a single-column configuration against observational data of oceanic convection from the LION buoy.

Even if the proposed derivation may seem tedious, the energetically consistent parameterization obtained is rather simple to implement, whether in a code with an existing "non-energetically consistent" EDMF scheme or, more generally, in any code relying on a prognostic TKE equation. The MF terms are obtained by solving a straightforward system of ODEs and take the form of vertical advection terms in the mean equations (see Appendix F for practical details). The proposed approach can also be applied in the case where the ED closure does not use TKE. In this case, it would require to add a prognostic or diagnostic TKE equation (even if it does not interact with the ED term) to enforce energetic consistency.

This paper was intentionally oriented toward the theoretical description of energetically consistent EDMF schemes. The first idealized test cases were not conclusive on several new aspects which should be further assessed using more realistic SCM/LES intercomparisons in future studies. Among these aspects, we can mention: the impact of choosing the total TKE k instead of the environmental TKE k_e to compute eddy-diffusivities (sec. 2.3.3); the impact of relaxing the small-area assumption presented in Appendix A; the impact of energetic consistency on the accuracy of the mean fields.

The development of energetically consistent EDMF schemes can be continued in several ways. First, for real-world applications, the present work has to be extended to more complex thermodynamics models (i.e. moist atmosphere, Pauluis (2008), and seawater with a non-linear equation of state, Tailleux and Dubos (2023)). As a starting point, we provided in Appendix E a derivation of EDMF energy budgets in the anelastic setting from a dry atmosphere. The proposed framework is flexible enough to be readily extended to other coherent structures of the boundary layer contributing to transport, such as atmospheric downdraft (Han & Bretherton, 2019; Brient et al., 2023). For atmospheric models, the ED-based Monin-Obukhov similarity theory should be reconciled with the EDMF representation of fluxes (Li et al., 2021) to provide unambiguous and consistent boundary conditions and thus avoid potential spurious boundary energy fluxes.

$\tilde{\alpha} = \frac{1}{1 - a_p}$	Rescaling coefficient
$\frac{\overline{w'\phi'}}{\overline{w'\mathbf{u}'_h}} = \tilde{\alpha} a_p w_p (\phi_p - \bar{\phi}) - K_\phi \partial_z \bar{\phi}$	Vertical turbulent flux for component ϕ
$\frac{\overline{w'\mathbf{u}'_h}}{\overline{w'\mathbf{u}'_h}} = \tilde{\alpha} a_p w_p (\mathbf{u}_{h,p} - \bar{\mathbf{u}}_h) - K_m \partial_z \bar{\mathbf{u}}_h$	Vertical turbulent momentum flux
$\partial_z(a_p w_p) = E - D$	Plume area conservation equation
$a_p w_p \partial_z \phi_p = \tilde{\alpha} E (\bar{\phi} - \phi_p)$	Plume equation for component ϕ
$a_p w_p \partial_z \mathbf{u}_{h,p} = \tilde{\alpha} E (\bar{\mathbf{u}}_h - \mathbf{u}_{h,p}) + a_p w_p C_u \partial_z \bar{\mathbf{u}}_h$	Plume horizontal momentum equation
$a_p w_p \partial_z w_p = -(\tilde{\alpha} b) E w_p + a_p \{a B_p - \sigma_o^a (\tilde{\alpha} b') w_p^2\}$	Plume vertical velocity equation
$B_p = b_{\text{eos}}(\phi_p) - b_{\text{eos}}(\bar{\phi})$	Buoyancy forcing term
$\partial_t k - \partial_z (K_k \partial_z k) = K_m (\partial_z \bar{\mathbf{u}}_h)^2 - K_\phi \partial_z \bar{b}$	ED related TKE production terms
$\quad - \tilde{\alpha} a_p w_p ((\mathbf{u}_{h,p} - \bar{\mathbf{u}}_h) \cdot \partial_z \bar{\mathbf{u}}_h - (b_p - \bar{b}))$	MF related TKE production terms
$\quad - \partial_z \left(\tilde{\alpha} a_p w_p \left[k_p - k + \frac{1}{2} \ \mathbf{u}_p - \mathbf{u}\ ^2 \right] \right)$	MF related TKE transport term
$\quad - \bar{\epsilon}_\nu$	TKE dissipation
$a_p w_p \partial_z k_p = \tilde{\alpha} E \left((k - k_p) + \frac{1}{2} \ \mathbf{u}_p - \mathbf{u}\ ^2 \right) - a_p (\epsilon_\nu)_p$	Plume related TKE

Table A1: Same as table 1, but with a relaxation of the small area limit. Note that under the small area limit we would have $\tilde{\alpha} \equiv 1$.

805 To implement and then assess the impact of this energetically consistent param-
 806 eterization on realistic 3D oceanic simulations a calibration of the remaining "free" pa-
 807 rameters must be achieved (Hourdin et al., 2017; Couvreur et al., 2021). It should be
 808 performed on parameters whose universality can sometimes be statistically assessed (Souza
 809 et al., 2020), and should be mathematically and physically constrained as much as pos-
 810 sible (see e.g. section 4.6). We believe that designing energetically consistent parame-
 811 terization is a way to achieve more realistic models before their tuning.

812 Appendix A Relaxing the small area limit

813 The small-area assumption can be relaxed with no additional complexity if the sub-
 814 plume fluxes $\overline{w'_p \phi'_p}$ are still neglected. A summary of the EDMF-Energy parameteriza-
 815 tion in such a regime is presented in Tab. A1.

816 Appendix B Mixing length computations

817 For the oceanic applications detailed in this article, we have chosen a formulation
 818 of eddy-diffusivity and viscosity close to that used in the NEMO ocean model (Madec
 819 et al., 2019). The eddy-viscosity and diffusivity are classically assumed to be related to
 820 TKE by

$$\begin{aligned} K_u &= c_m l_m \sqrt{k} \\ K_\phi &= K_u (\text{Pr}_t)^{-1} \end{aligned}$$

821 with l_m a mixing length scale, Pr_t the non-dimensional turbulent Prandtl number, and
 822 c_m is a constant ($c_m = 0.1$ in NEMO). The mixing length l_m is calculated in two steps
 823 by considering separately the length scales l_{up} and l_{dwn} associated respectively to up-
 824 ward and downward movements : (1) l_{up} and l_{dwn} are initialized assuming $l_{\text{up}} = l_{\text{dwn}} =$

825 $\sqrt{2k}\tau_{ed}$ with τ_{ed} a characteristic time equal to $1/N = (\partial_z \bar{b})^{-1}$ (2) a physical limitation
 826 is used to guarantee that l_{up} and l_{dwn} do not exceed the distance to the top and the bot-
 827 tom, this limitation amounts to controlling the vertical gradients of l_{up} and l_{dwn} such
 828 that they are not larger than the variations of depth (*e.g.* Madec et al., 2019). Once l_{up}
 829 and l_{dwn} are computed the mixing length is taken as $l_m = \min(l_{up}, l_{dwn})$. The turbu-
 830 lent Prandtl number is modelled by $Pr_t = \min(Pr_t^{max}, \max(Ri/Ri_c, 1))$ with $Ri = N^2/\|\partial_z \bar{\mathbf{u}}_h\|^2$,
 831 $Pr_t^{max} = 10$ and $Ri_c = 0.2$.

832 Appendix C Boundary condition for plume equations

833 Near the surface, we linearize the plume and mean buoyancy in the form $b \simeq b^0 +$
 834 $b'z$. Then the plume equation for b_p reads at order $O(z^0)$:

$$a_p^0 w_p^0 b'_p = -E_0 (b_p^0 - \bar{b}^0)$$

835 The boundary condition $b_p^0 = \bar{b}^0$ implies that $b'_p = 0$. Thus we get

$$b_p(z) \simeq \bar{b}^0, \quad \bar{b} \simeq \bar{b}^0 + N_0^2 z$$

836 Then near the surface, the buoyancy force - which is a source of plume momentum and
 837 kinetic energy $1/2 w_p^2$ - is at first order $b_p - \bar{b} \simeq -N_0^2 z$. Consequently, any static insta-
 838 bility at the surface will result in the absolute growth of the plume vertical momentum
 839 ($-N_0^2 z > 0$ in the atmosphere and $-N_0^2 z < 0$ in the ocean).

840 The boundary condition $b_p(0) = \bar{b}(0)$ implies that at $z = 0$, all the surface flux is al-
 841 located in the ED component. Consequently, $N_0^2 = \overline{w'b'}(0)/(-K_b(0)) = \overline{w'b'}(0)/(c_b l_b(0) \sqrt{k(0)})$.
 842 The boundary condition $b_p(0) = \bar{b}(0)$ thus implies that close to the surface

$$b_p(z) \simeq \bar{b}(z) + \frac{\overline{w'b'}(0)}{c_b l_b(0) \sqrt{k_0}} z$$

843 Appendix D EDMF Mean Variance Equation

844 Start from the mean and plume equations, and the turbulent flux decomposition

$$\partial_t \bar{X} = -\partial_z \overline{w'X'} + \bar{S}_X \tag{D1}$$

$$\overline{w'X'} = -K_X \partial_z \bar{X} + a_p w_p (X_p - \bar{X}) \tag{D2}$$

$$a_p w_p \partial_z X_p = -E(X_p - \bar{X}) + a_p S_{X,p} \tag{D3}$$

845 Multiplying the mean equation (D1) by \bar{X} leads to

$$\begin{aligned} \frac{1}{2} \partial_t \bar{X}^2 &= -\partial_z (\bar{X} \overline{w'X'}) + \overline{w'X'} \partial_z \bar{X} + \bar{X} \bar{S}_X \\ &= -\partial_z (\bar{X} \overline{w'X'}) - K_X (\partial_z \bar{X})^2 + a_p w_p (X_p - \bar{X}) \partial_z \bar{X} + \bar{X} \bar{S}_X \end{aligned} \tag{D4}$$

846 To rewrite the second term of the right-hand side, we use the plume equation (D2):

$$\begin{aligned}
 a_p w_p (X_p - \overline{X}) \partial_z \overbrace{X}^{=X_p + (\overline{X} - X_p)} &= -E(X_p - \overline{X})^2 + (X_p - \overline{X}) a_p S_{X,p} \\
 &\quad - a_p w_p \frac{1}{2} \partial_z (X_p - \overline{X})^2 \\
 &= -E(X_p - \overline{X})^2 + (X_p - \overline{X}) a_p S_{X,p} \\
 &\quad - \partial_z (a_p w_p \frac{1}{2} (X_p - \overline{X})^2) \\
 &\quad + (E - D) \frac{1}{2} (X_p - \overline{X})^2 \\
 &= -(E + D) \frac{1}{2} (X_p - \overline{X})^2 + (X_p - \overline{X}) a_p S_{X,p} \\
 &\quad - \partial_z (a_p w_p \frac{1}{2} (X_p - \overline{X})^2)
 \end{aligned}$$

847 Using this expression into equation (D4), then vertically integrating the variance bud-
 848 get leads to the desired equation (71).

849 Appendix E Anelastic energy budgets

850 In this appendix, we derive energy budgets for a general anelastic model commonly
 851 used in atmospheric models. We start with the unaveraged anelastic mass and momen-
 852 tum budgets:

$$\nabla \cdot (\rho_{\text{ref}} \mathbf{u}) = 0 \quad (\text{E1})$$

$$\partial_t \mathbf{u} = -\nabla \cdot (\mathbf{u} \otimes \mathbf{u}) - \mathbf{f} \times \mathbf{u} - \nabla \left(\frac{p^\dagger}{\rho_{\text{ref}}} \right) + b \mathbf{e}_z + \nu \nabla^2 \mathbf{u} \quad (\text{E2})$$

853 where $\rho_{\text{ref}} = \rho_{\text{ref}}(z)$ is a reference density profile, and the total pressure is $p(x, y, z, t) =$
 854 $p_{\text{ref}}(z) + p^\dagger(x, y, z, t)$ where by definition $\partial_z p_{\text{ref}}(z) = -\rho_{\text{ref}} g$.

855 As in section 3, we keep the same notations for the specific mean kinetic energy
 856 $E_k = (\overline{\mathbf{u}_h} \cdot \overline{\mathbf{u}_h})/2$, the turbulent kinetic energy $k = (\overline{\mathbf{u}' \cdot \mathbf{u}'})/2$, the potential energy
 857 $E_p = gz$ and the mean internal energy E_i . Note however that these *specific energies*
 858 have to be multiplied by ρ_{ref} to get corresponding energies.

859 E1 Kinetic energies

860 By using the SCM assumptions exposed in Sec. 2.1, we can derive budgets for the
 861 resolved kinetic energy E_k and the turbulent kinetic energy k :

$$\partial_t E_k + \frac{1}{\rho_{\text{ref}}} \partial_z T_{E_k} = \overline{w' \mathbf{u}'_h} \cdot \partial_z \overline{\mathbf{u}_h} \quad (\text{E3})$$

$$\partial_t k + \frac{1}{\rho_{\text{ref}}} \partial_z T_k = -\overline{w' \mathbf{u}'_h} \cdot \partial_z \overline{\mathbf{u}_h} + \overline{w' b'} - \overline{\epsilon}_\nu \quad (\text{E4})$$

862 where $\overline{\epsilon}_\nu = \nu \overline{\partial_z \mathbf{u}' \cdot \partial_z \mathbf{u}'}$ is the viscous dissipation of energy, $T_{E_k} = \rho_{\text{ref}} \overline{w' \mathbf{u}'_h} \cdot \overline{\mathbf{u}_h}$ and
 863 $T_k = \rho_{\text{ref}} \overline{w' \frac{\mathbf{u}' \cdot \mathbf{u}'}{2} + w' p^\dagger}$. Exchanges between the resolved and subgrid reservoirs of ki-
 864 netic energy are done via the mechanical shear term $\overline{w' \mathbf{u}'_h} \cdot \partial_z \overline{\mathbf{u}_h}$. To close the budgets,
 865 we will provide in the following sections a budget of internal and potential energy.

866 E2 Internal and Potential energies

867 For a generic fluid, the unaveraged specific internal energy can be written as

$$\mathcal{E}_i = \mathfrak{h}(p, \phi) - \frac{p}{\rho} \quad (\text{E5})$$

868 where h is the specific enthalpy and ϕ is any entropic variable describing each compo-
869 nent of the fluid. Within the context of anelastic approximation, internal energy becomes

$$\mathcal{E}_i = h(p_{\text{ref}}, \phi) - \frac{p_{\text{ref}}}{\rho_{\text{ref}}} \quad (\text{E6})$$

870 In particular, it implies within the anelastic approximation that $b(\phi) := -g(\rho(p_{\text{ref}}, \phi) -$
871 $\rho_{\text{ref}})/\rho(p_{\text{ref}}, \phi)$, where the specific volume can be defined as $1/\rho(p_{\text{ref}}, \phi) = \partial_p h(p_{\text{ref}}, \phi)$.
872 The unaveraged budget of internal and potential energy then reads

$$\partial_t(\mathcal{E}_i + E_p) + \frac{1}{\rho_{\text{ref}}} \nabla \cdot [\rho_{\text{ref}}(h(p_{\text{ref}}, \phi) + gz)\mathbf{u}] = \epsilon_\nu - wb \quad (\text{E7})$$

873 Upon averaging and using the SCM assumptions, the budget of mean internal energy
874 $E_i = \bar{\mathcal{E}}_i$ and potential energy reads

$$\partial_t(E_i + E_p) + \frac{1}{\rho_{\text{ref}}} \partial_z(\rho_{\text{ref}} \overline{\partial_\phi h_{\text{ref}} w' \phi'}) = \bar{\epsilon}_\nu - \frac{1}{\rho_{\text{ref}}} \partial_z(\rho_{\text{ref}} (\bar{\phi} \overline{w' \partial_\phi h'_{\text{ref}}} + \overline{\phi' w' \partial_\phi h'_{\text{ref}}})) - \overline{w' b'} \quad (\text{E8})$$

875 where we introduced the notation $\overline{h_{\text{ref}}(\phi)} = h(p_{\text{ref}}, \phi)$. Remark that if $h(p_{\text{ref}}, \phi)$ is lin-
876 ear in ϕ , we have closed relations $\overline{h(p_{\text{ref}}, \phi)} = h(p_{\text{ref}}, \bar{\phi})$ and $\overline{b(\phi)} = b(\bar{\phi})$.

877 As a summary, the budgets of mean kinetic energy, turbulent kinetic energy and
878 the sum of mean internal and potential energy are

$$\begin{cases} \partial_t E_k + \partial_z T_{E_k} & = \overline{w' \mathbf{u}'_h} \cdot \partial_z \bar{\mathbf{u}}_h \\ \partial_t k + \partial_z T_k & = -\overline{w' \mathbf{u}'_h} \cdot \partial_z \bar{\mathbf{u}}_h + \overline{w' b'} - \bar{\epsilon}_\nu \\ \partial_t(E_i + E_p) + \frac{1}{\rho_{\text{ref}}} \partial_z(\rho_{\text{ref}} \overline{\partial_\phi h_{\text{ref}} w' \phi'}) & = \bar{\epsilon}_\nu - \frac{1}{\rho_{\text{ref}}} \partial_z(\rho_{\text{ref}} \bar{\phi} \overline{w' \partial_\phi h'_{\text{ref}}} + \overline{\phi' w' \partial_\phi h'_{\text{ref}}}) - \overline{w' b'} \end{cases} \quad (\text{E9})$$

879 where conversion of E_k into k occurs via mean shear, conversion of k into E_i occurs via
880 viscous dissipation, and conversion of k into $E_i + E_p$ occurs via buoyancy fluxes.

881 For a *dry atmosphere* modeled as an ideal gas $p = \rho R_d T$, the specific enthalpy
882 reads

$$h(p_{\text{ref}}, \theta) = c_p \left(\frac{p_{\text{ref}}}{p_0} \right)^{R_d/c_p} \theta \quad (\text{E10})$$

883 which is linear in the potential temperature $\theta = T (p/p_0)^{-R_d/c_p}$. and buoyancy is $b(\bar{\theta}) =$
884 $g(\bar{\theta} - \theta_{\text{ref}})/\theta_{\text{ref}}$. The budget of $E_i + E_p$ is

$$\partial_t(E_i + E_p) = c_p \left(\frac{p_{\text{ref}}}{p_0} \right)^{R_d/c_p} \partial_t \bar{\theta} = \bar{\epsilon}_\nu - \frac{1}{\rho_{\text{ref}}} \partial_z \left(\rho_{\text{ref}} c_p \left(\frac{p_{\text{ref}}}{p_0} \right)^{R_d/c_p} \overline{w' \theta'} \right) - \frac{g}{\theta_{\text{ref}}} \overline{w' \theta'} \quad (\text{E11})$$

885 where $\theta_{\text{ref}} = \left(\frac{p_{\text{ref}}}{p_0} \right)^{-R_d/c_p} \frac{p_{\text{ref}}}{\rho_{\text{ref}} R_d}$. As a summary, the budgets of mean kinetic energy,
886 turbulent kinetic energy and the sum of mean internal and potential energy for a *dry at-*
887 *mosphere* within the anelastic approximation are

$$\begin{cases} \partial_t E_k + \partial_z T_{E_k} & = \overline{w' \mathbf{u}'_h} \cdot \partial_z \bar{\mathbf{u}}_h \\ \partial_t k + \partial_z T_k & = -\overline{w' \mathbf{u}'_h} \cdot \partial_z \bar{\mathbf{u}}_h + \frac{g}{\theta_{\text{ref}}} \overline{w' \theta'} - \bar{\epsilon}_\nu \\ c_p \left(\frac{p_{\text{ref}}}{p_0} \right)^{R_d/c_p} \partial_t \bar{\theta} & = \bar{\epsilon}_\nu - \frac{1}{\rho_{\text{ref}}} \partial_z \left(\rho_{\text{ref}} c_p \left(\frac{p_{\text{ref}}}{p_0} \right)^{R_d/c_p} \overline{w' \theta'} \right) - \frac{g}{\theta_{\text{ref}}} \overline{w' \theta'} \end{cases} \quad (\text{E12})$$

888 E3 EDMF-parameterized budget

889 Within the anelastic approximation, the budget of resolved kinetic energy, subgrid
890 kinetic energy and resolved internal+potential energy for a *dry atmosphere* with EDMF

891 closures is

$$\begin{cases} \partial_t E_k + \frac{1}{\rho_{\text{ref}}} \partial_z T_{E_k} & = -K_u (\partial_z \bar{\mathbf{u}}_h)^2 + a_p w_p (\mathbf{u}_{h,p} - \bar{\mathbf{u}}_h) \cdot \partial_z \bar{\mathbf{u}}_h \\ \partial_t k + \frac{1}{\rho_{\text{ref}}} \partial_z T_k & = \frac{g}{\theta_{\text{ref}}} [-K_\theta \partial_z \bar{\theta} + a_p w_p (\theta_p - \bar{\theta})] + K_u (\partial_z \bar{\mathbf{u}}_h)^2 - a_p w_p (\mathbf{u}_{h,p} - \bar{\mathbf{u}}_h) \cdot \partial_z \bar{\mathbf{u}}_h - \bar{\epsilon}_\nu \\ \partial_t \left[c_p \left(\frac{p_{\text{ref}}}{p_0} \right)^{R_d/c_p} \bar{\theta} \right] & = -\frac{1}{\rho_{\text{ref}}} \partial_z T_{E_i+E_p} + \bar{\epsilon}_\nu - \frac{g}{\theta_{\text{ref}}} [-K_\theta \partial_z \bar{\theta} + a_p w_p (\theta_p - \bar{\theta})] \end{cases} \quad (\text{E13})$$

892 where the flux terms are

$$T_{E_k} = \rho_{\text{ref}} (-K_u \partial_z \bar{\mathbf{u}}_h + a_p w_p (\mathbf{u}_{h,p} - \bar{\mathbf{u}}_h)) \cdot \bar{\mathbf{u}}_h \quad (\text{E14})$$

$$T_k = -\rho_{\text{ref}} K_k \partial_z k + \rho_{\text{ref}} a_p w_p \left(k_p - k + \frac{1}{2} \|\mathbf{u}_p - \bar{\mathbf{u}}\|^2 \right) \quad (\text{E15})$$

$$T_{E_i+E_p} = \rho_{\text{ref}} c_p \left(\frac{p_{\text{ref}}}{p_0} \right)^{R_d/c_p} (-K_\theta \partial_z \bar{\theta} + a_p w_p (\theta_p - \bar{\theta})) \quad (\text{E16})$$

893 Appendix F Discretization of energetically consistent EDMF equa- 894 tions

895 We start from the standard grid arrangement used in oceanic models which are usu-
896 ally discretized on a Lorenz grid in the vertical (density is located in the center of the
897 cells on the vertical). We consider N grid cells in the vertical with thickness $\Delta z_j = z_{j+1/2} -$
898 $z_{j-1/2}$ ($z_{1/2} = -H$ and $z_{N+1/2} = 0$ the surface) such that $\sum_{j=1}^N \Delta z_j = -H$. Tradi-
899 tionally, the turbulent quantities like turbulent kinetic energy k and eddy diffusivities
900 K_X are naturally located on the interfaces at $z_{j+1/2}$ to avoid interpolations when com-
901 puting the vertical gradients of the turbulent fluxes (Burchard, 2002). For the discrete
902 values, not to interfere with the grid indices, the subscript p for the plume quantities is
903 now a superscript such that plume quantities are now noted $X_{j+1/2}^p = X_p(z = z_{j+1/2})$.
904 In the following, we consider that the plume quantities and k are discretized at cell in-
905 terfaces and the mean quantities \bar{X} are discretized at cell centers and are interpreted in
906 a finite-volume sense (i.e. $\bar{X}_j = \frac{1}{\Delta z_j} \int_{z_{j-1/2}}^{z_{j+1/2}} \bar{X}(z) dz$). In the remainder, we consider
907 the oceanic case with $\sigma_o^a = -1$.

908 F1 Discretization of mass-flux equations

909 We consider here the mass-flux equations given in Tab. 1 but in conservative form
910 (except for the vertical velocity and TKE plume equations) :

$$\partial_z (a_p w_p) = E - D \quad (\text{F1})$$

$$\partial_z (a_p w_p \phi_p) = E \bar{\phi} - D \phi_p \quad (\text{F2})$$

$$\partial_z (a_p w_p \mathbf{U}_p) = E \bar{\mathbf{U}} - D \mathbf{U}_p \quad (\text{F3})$$

$$w_p \partial_z w_p = -(E/a_p) (b w_p) + a B_p + b' w_p^2 \quad (\text{F4})$$

$$a_p w_p \partial_z k_p = E \left(k - k_p + \frac{1}{2} (\bar{\mathbf{u}}_p - \bar{\mathbf{u}})^2 \right) - a_p (\epsilon_\nu)_p \quad (\text{F5})$$

911 where the equation for horizontal momentum has been manipulated to have the same
912 form as the ϕ_p equation by taking $\mathbf{U}_p = \mathbf{u}_{h,p} - C_u \bar{\mathbf{u}}_h$ and $\bar{\mathbf{U}} = (1 - C_u) \bar{\mathbf{u}}_h$. The ad-
913 vective form is used for the w_p equation to make the computation of w_p independent of
914 a_p (with the closure hypothesis (25) for E , E/a_p is independent of a_p); the motivations
915 for this will become clearer later. The mass-flux equations correspond to a first-order
916 nonlinear set of ODEs. There are a whole lot of methods for solving such initial value
917 problems. We present here a simple method combining explicit (Euler) and semi-implicit
918 (Crank-Nicolson) steps as the use of more advanced methods did not produce significantly
919 different results. In the following, we describe the different steps for the resolution start-
920 ing from known initial values $X_{N+1/2}^p$ at the surface and advancing downward.

921 **F11 Initial conditions**

922 The discrete form of the initial conditions given in 2.4 are obtained by a linear ex-
 923 trapolation of $\bar{\phi}_N$ and $(\bar{\mathbf{u}}_h)_N$ toward the surface.

$$\begin{aligned} w_{N+1/2}^p &= -w_{\min}^p \\ \phi_{N+1/2}^p &= \frac{(2\Delta z_N + \Delta z_{N-1})\bar{\phi}_N - \Delta z_N \bar{\phi}_{N-1}}{\Delta z_N + \Delta z_{N-1}} \\ \mathbf{U}_{N+1/2}^p &= (1 - C_u) \frac{(2\Delta z_N + \Delta z_{N-1})(\bar{\mathbf{u}}_h)_N - \Delta z_N (\bar{\mathbf{u}}_h)_{N-1}}{\Delta z_N + \Delta z_{N-1}} \end{aligned} \quad (\text{F6})$$

924 Since the TKE k is already discretized at cell interfaces the boundary condition for k_p
 925 does not require an extrapolation. In particular the condition on ϕ_p leads to the follow-
 926 ing value of the B_p term in the topmost grid cell :

$$B_N^p = \Delta z_N \left(\frac{\bar{b}_N - \bar{b}_{N-1}}{\Delta z_N + \Delta z_{N-1}} \right) = \frac{\Delta z_N}{2} (N^2)_{N-1/2}$$

927 meaning that using the condition (F6) allows to trigger convection as soon as the Brunt-
 928 Väisälä frequency is negative. Indeed a negative value of B_N^p in the RHS of the w_p -equation
 929 (F4) leads to a positive value of $(\partial_z w_p)_N$ and thus larger negative values of w_p when go-
 930 ing downward.

931 **F12 w_p -equation**

932 The w_p -equation (F4) using the entrainment E given in (25) can be formulated as

$$\partial_z w_p^2 + b\beta_1 \min(\partial_z w_p^2, 0) = 2aB_p + 2b'w_p^2$$

933 which can be discretized in a straightforward way as

$$\begin{aligned} \tilde{\beta} \left[(w^p)_{j+1/2}^2 - (w^p)_{j-1/2}^2 \right] &= 2a\Delta z_j B_j^p - \sigma_o^a (b' \Delta z_j) \left[(w^p)_{j+1/2}^2 + (w^p)_{j-1/2}^2 \right] \\ B_j^p &= b_{\text{eos}}(\phi_{j+1/2}^p) - b_{\text{eos}}(\bar{\phi}_j) \end{aligned} \quad (\text{F7})$$

934 where $\tilde{\beta} = 1 + b\beta_1$ if $aB_j^p - \sigma_o^a (b' \Delta z_j) (w^p)_{j+1/2}^2$ is negative and $\tilde{\beta} = 1$ otherwise. Knowing
 935 $w_{j+1/2}^p$, it is easily found that

$$(w^p)_{j-1/2}^2 = \frac{(\tilde{\beta} - b' \Delta z_j)(w^p)_{j+1/2}^2 - 2a\Delta z_j B_j^p}{\tilde{\beta} + b' \Delta z_j}$$

936 Once this quantity falls below a certain threshold $(w_{\min}^p)^2$, the plume is considered evanes-
 937 cent. In the oceanic context we consider $w_{j-1/2}^p = -\sqrt{(w^p)_{j-1/2}^2}$ for the rest of the cal-
 938 culations to guarantee that $w_{j-1/2}^p$ is strictly negative. The unwinding used to compute
 939 B_p in (F7) in addition to the fact that the w_p -equation does not depend on a_p avoid the
 940 need for an iterative process to solve the mass-flux equations.

941 **F13 Continuity and tracer equations**

942 The entrainment E_j and detrainment D_j rates given in (25) and (26) discretized
 943 on a grid cell j correspond to

$$\begin{aligned} \Delta z_j E_j &= \frac{1}{2} \left(a_{j+1/2}^p + a_{j-1/2}^p \right) \beta_1 (\delta_z w^p)_j^+ \\ \Delta z_j D_j &= \frac{1}{2} \left(a_{j+1/2}^p + a_{j-1/2}^p \right) \left[-\beta_2 (\delta_z w^p)_j^- - \frac{\delta_0 \Delta z_j}{2} (w_{j+1/2}^p + w_{j-1/2}^p) \right] \end{aligned}$$

944 where $(\delta_z w^p)_j^+ = \max(w_{j+1/2}^p - w_{j-1/2}^p, 0)$ and $(\delta_z w^p)_j^- = \min(w_{j+1/2}^p - w_{j-1/2}^p, 0)$.
 945 Integrating from $z_{j-1/2}$ to $z_{j+1/2}$ the continuity equation and ϕ_p equations we obtain

$$(a^p w^p)_{j+1/2} - (a^p w^p)_{j-1/2} = \Delta z_j (E_j - D_j)$$

$$(a^p w^p \phi^p)_{j+1/2} - (a^p w^p \phi^p)_{j-1/2} = \Delta z_j E_j \bar{\phi}_j - (\Delta z_j D_j / 2) (\phi_{j+1/2}^p + \phi_{j-1/2}^p)$$

946 which can also be extended to the horizontal momentum equation formulated using U_p .
 947 Since at this stage $w_{j+1/2}^p$ and $w_{j-1/2}^p$ are known, the continuity equation is used to com-
 948 pute $a_{j-1/2}^p$ through

$$a_{j-1/2}^p = a_{j+1/2}^p \left\{ \frac{2w_{j+1/2}^p - \text{EmD}_j}{2w_{j-1/2}^p + \text{EmD}_j} \right\}$$

$$\text{EmD}_j = \beta_1 (\delta_z w^p)_j^+ + \beta_2 (\delta_z w^p)_j^- + \min \left\{ \frac{\delta_0 \Delta z_j}{2} (w_{j+1/2}^p + w_{j-1/2}^p), -2(w_{\min}^p) \right\} \quad (\text{F8})$$

949 Note that a_p is subject to a boundedness requirement as $0 \leq a_p \leq 1$. Assuming $0 \leq$
 950 $a_{j+1/2}^p \leq 1$, sufficient conditions to guarantee that $a_{j-1/2}^p \leq 1$ are $\beta_1 \leq 1$ and $\beta_2 \geq$
 951 1 and a sufficient condition to guarantee that $a_{j-1/2}^p \geq 0$ is $\beta_2 < 2$. Moreover a con-
 952 straint is added on the background detrainment δ_0 in (F8) to guarantee that $a_{j-1/2}^p =$
 953 0 as soon as $w_{j+1/2}^p = w_{j-1/2}^p = -w_{\min}^p$ which occurs once outside the plume.

954 Once $a_{j-1/2}^p$ is known, it is possible to compute $\phi_{j-1/2}^p$ (as well as $U_{j-1/2}^p$). The
 955 proposed discretization ensures that the compatibility between the continuity and the
 956 tracer equations is maintained at the discrete level (*i.e.* we recover the continuity equa-
 957 tion for $\phi_{j+1/2}^p = \phi_{j-1/2}^p = 1$ and $\bar{\phi}_j = 1$).

958 The same reasoning can be applied to solve the k_p equation, which presents no ad-
 959 ditional difficulties as all necessary quantities $w_{j\pm 1/2}^p$, $a_{j\pm 1/2}^p$ and $u_{j\pm 1/2}^p$ are known.

960 In summary, the proposed discretization guarantees that w_p is strictly negative, that
 961 a_p is bounded between 0 and 1, and that the continuity and tracer equations are com-
 962 patible, without the need for an iterative solution procedure.

963 F2 Energy consistent discretization of turbulent kinetic energy

964 In Burchard (2002) an energetically consistent discretization of the turbulent shear
 965 and buoyancy production terms for the TKE equation in the ED case is derived. Such
 966 methodology can be extended in the EDMF case to discretize the MF-related TKE pro-
 967 duction terms given in magenta and cyan in Tab. 2. Starting from a simple Euler-upwind
 968 discretization of mass-flux terms in the \bar{u}_h and $\bar{\phi}$ equations which can be written gener-
 969 ically for a variable X

$$\frac{\bar{X}_j^{n+1} - \bar{X}_j^n}{\Delta t} = \frac{F_{j+1/2}^{\text{MF}} - F_{j-1/2}^{\text{MF}}}{\Delta z_j}$$

$$F_{j+1/2}^{\text{MF}} = (a^p w^p)_{j+1/2} (\bar{X}_{j+1/2}^p - \bar{X}_j^n)$$

970 the kinetic and potential energy budgets can be derived by multiplying the velocity equa-
 971 tions (*i.e.* $\bar{X} = u$) by $(\bar{u}_j^{n+1} + \bar{u}_j^n)/2$ and the buoyancy equation by $-z_j$. After some
 972 simple algebra, we obtain that

$$(a_p w_p (\mathbf{u}_{h,p} - \bar{\mathbf{u}}_h) \cdot \partial_z \bar{\mathbf{u}}_h)_{j+1/2} = (a_p w_p)_{j+1/2} \left((\mathbf{u}_h)_{j+1/2}^p - (\mathbf{u}_h)_j^n \right) \cdot \left(\frac{(\mathbf{u}_h)_{j+1}^{n+1} + (\mathbf{u}_h)_{j+1}^n - (\mathbf{u}_h)_j^{n+1} - (\mathbf{u}_h)_j^n}{2\Delta z_{j+1/2}} \right)$$

$$(a_p w_p (b_p - \bar{b}))_{j+1/2} = (a_p w_p)_{j+1/2} B_j^p$$

973 where B_j^p is given in (F7). Using these discrete forms for the MF-related TKE produc-
 974 tion terms combined with the discretization of the turbulent shear and buoyancy pro-

duction terms derived in Burchard (2002) ensure the proper energy flux between resolved and subgrid energies.

F3 Coupling ED and MF schemes

In the EDMF approach, the usual vertical diffusion/viscous subgrid terms are completed by an advective term so that the following equation must be advanced in time:

$$\partial_t \bar{X} = \partial_z (K_X \partial_z \bar{X}) - \partial_z (a_p w_p (X^p - \bar{X})) \quad (\text{F9})$$

This amounts to couple a boundary layer scheme which provides K_X and a convection scheme which provides $a_p w_p$ and X^p . The numerical treatment of such coupling is rarely discussed in the literature. This problem can be approached in 2 ways: either by integrating the 2 schemes sequentially or in parallel. For the numerical experiments discussed in Sec. 5 we chose a *boundary layer-then-convection* strategy corresponding to the following temporal integration for the single-column model (leaving aside the Coriolis and solar penetration terms)

ED step

$$\begin{aligned} \phi^{n+1,*} &= \phi^n + \Delta t \partial_z (K_\phi(k^n, b^n) \partial_z \phi^{n+1,*}) \\ \mathbf{u}_h^{n+1,*} &= \mathbf{u}_h^n + \Delta t \partial_z (K_u(k^n, b^n) \partial_z \mathbf{u}_h^{n+1,*}) \\ b^{n+1,*} &= b_{\text{eos}}(\phi^{n+1,*}) \end{aligned}$$

MF step

$$\begin{aligned} [a_p, w_p, \phi_p, \mathbf{u}_{h,p}, k_p, B_p] &= \text{MF}(b^{n+1,*}, \mathbf{u}_h^{n+1,*}) \\ \phi^{n+1} &= \phi^{n+1,*} - \Delta t \partial_z (a_p w_p (\phi_p - \phi^{n+1,*})) \\ \mathbf{u}_h^{n+1} &= \mathbf{u}_h^{n+1,*} - \Delta t \partial_z (a_p w_p (\mathbf{u}_{h,p} - \mathbf{u}_h^{n+1,*})) \end{aligned}$$

TKE update

$$k^{n+1} = k^n + \Delta t \partial_z (K_k(k^n, b^n) \partial_z k^{n+1}) + \mathcal{F}_k(b^{n+1}, \mathbf{u}_h^{n+1}, \mathbf{u}_h^n, a_p, w_p, \mathbf{u}_{h,p}, k_p, B_p)$$

where the $\text{MF}(\cdot)$ function represents the computation of mass-flux quantities as described previously and \mathcal{F}_k contains the TKE transport and forcing terms. The "ED step" is classically computed using an Euler backward scheme. With the proposed approach, the convection scheme sees a state already updated by the boundary layer scheme (and by the solar penetration and non-solar surface heat flux which are applied during the "ED step") The convection scheme thus sees a state whose static stability is representative of the current time-step and external forcing.

Ultimately, with the proposed approach, the various stages can be expressed directly as follows

$$\begin{aligned} \phi^{n+1} &= \phi^n + \Delta t \partial_z (K_\phi \partial_z \phi^{n+1,*} - a_p w_p (\phi_p - \phi^{n+1,*})) \\ [a_p, w_p, \phi_p] &= \text{MF}(\phi^{n+1,*}) \end{aligned}$$

which reflects the fact that we have good synchronization between the ED part and the MF part, which see the same mean fields. On the other hand, the approach of simultaneously considering the ED and MF parts in a single tridiagonal problem would lead to

$$\begin{aligned} \phi^{n+1} &= \phi^n + \Delta t (K_\phi \partial_z \phi^{n+1} - a_p w_p (\phi_p - \phi^{n+1})) \\ [a_p, w_p, \phi_p] &= \text{MF}(\phi^n) \end{aligned}$$

In this case, the mass flux is applied to the mean fields at time n thus breaking the synchronization between the ED and MF parts. Indeed ϕ_p has been computed using ϕ^n while it is applied at time $n + 1$.

Open Research

Data Availability Statement

Data from the Lion mooring (located in the Gulf of Lion; Mediterranean sea) are freely accessible from Bosse et al. (2023). The output from LES simulations and the initial and surface boundary conditions for the Hymex/ASICS-MED experiments are available at the Zenodo archive 10.5281/zenodo.10619442.

Software Availability Statement

All the numerical codes used in this study have been made available and can be found at the Zenodo archive 10.5281/zenodo.10619442. It includes the single-column model with Eddy-Diffusivity Mass-Flux turbulent closure developed from scratch. The latter consists of low-level code written in Fortran interfaced with Python using F2PY (Peterson, 2009). The single-column simulations analyzed in this study can be executed from a high-level Python driver code without any intervention on the Fortran code. The high-level Python driver code and scripts to reproduce the figures are available in the Zenodo archive. The Fortran code contains inline documentation following the FORD (Fortran Documenter) format.

Acknowledgments

This work was supported by the *institut des Mathématiques pour la Planète Terre* (iMPT) through the project "Coherent sub-grid scale modeling for ocean climate models". This study was carried out as part of the technological defense project PROTEVS2 under the auspices of the French Ministry of the Armies / DGA. MP was supported by a PhD fellowship from Ecole Normale Supérieure Paris. The authors are extremely grateful to Jean-Luc Redelsperger for his essential contributions to the MESO-NH model and Thomas Dubos for constructive comments on an earlier version of this paper. This research was funded in part by l'Agence Nationale de la Recherche (ANR), project ANR-23-CE01-0009.

References

- Arakawa, A., & Schubert, W. H. (1974). Interaction of a Cumulus Cloud Ensemble with the Large-Scale Environment, Part I. *J. Atmos. Sci.*, *31*(3), 674–701. doi: 10.1175/1520-0469(1974)031<0674:IOACCE>2.0.CO;2
- Bony, S., Stevens, B., Frierson, D. M. W., Jakob, C., Kageyama, M., Pincus, R., . . . Webb, M. J. (2015). Clouds, circulation and climate sensitivity. *Nat. Geosci.*, *8*(4), 261–268. doi: 10.1038/ngeo2398
- Bosse, A., Testor, P., Coppola, L., Bretel, P., Dausse, D., Durrieu de Madron, X., . . . D'ortenzio, F. (2023). *LION observatory data*. Retrieved from <https://doi.org/10.17882/44411> (Type: Dataset) doi: 10.17882/44411
- Bretherton, C. S., McCaa, J. R., & Grenier, H. (2004, April). A New Parameterization for Shallow Cumulus Convection and Its Application to Marine Subtropical Cloud-Topped Boundary Layers. Part I: Description and 1D Results. *Monthly Weather Review*, *132*(4), 864–882. Retrieved from https://journals.ametsoc.org/view/journals/mwre/132/4/1520-0493_2004_132_0864_anpfsc_2.0.co_2.xml doi: 10.1175/1520-0493(2004)132<0864:ANPFSC>2.0.CO;2
- Brient, F., Couvreur, F., Rio, C., & Honnert, R. (2023). Coherent subsiding structures in large eddy simulations of atmospheric boundary layers. *Quart. J. Roy. Meteorol. Soc.* doi: 10.1002/qj.4625

- 1049 Burchard, H. (2002). Energy-conserving discretisation of turbulent shear and buoy-
 1050 ancy production. *Ocean Modell.*, 4(3-4), 347–361. doi: 10.1016/S1463-5003(02)
 1051 00009-4
- 1052 Coppola, L., Prieur, L., Taupier-Letage, I., Estournel, C., Testor, P., Lefevre, D.,
 1053 ... Taillandier, V. (2017). Observation of oxygen ventilation into deep
 1054 waters through targeted deployment of multiple argo-o2 floats in the north-
 1055 western mediterranean sea in 2013. *J. Geophys. Res.*, 122(8), 6325-6341. doi:
 1056 https://doi.org/10.1002/2016JC012594
- 1057 Couvreur, F., Guichard, F., Masson, V., & Redelsperger, J.-L. (2007). Negative
 1058 water vapour skewness and dry tongues in the convective boundary layer: ob-
 1059 servations and large-eddy simulation budget analysis. *Bound.-Lay. Meteorol.*,
 1060 123(2), 269–294. doi: 10.1007/s10546-006-9140-y
- 1061 Couvreur, F., Hourdin, F., & Rio, C. (2010, March). Resolved Versus Parametrized
 1062 Boundary-Layer Plumes. Part I: A Parametrization-Oriented Conditional
 1063 Sampling in Large-Eddy Simulations. *Boundary-Layer Meteorology*,
 1064 134(3), 441–458. Retrieved 2022-02-21, from [https://doi.org/10.1007/
 1065 s10546-009-9456-5](https://doi.org/10.1007/s10546-009-9456-5) doi: 10.1007/s10546-009-9456-5
- 1066 Couvreur, F., Hourdin, F., Williamson, D., Roehrig, R., Volodina, V., Villefranche,
 1067 N., ... Xu, W. (2021). Process-Based Climate Model Development Harnessing
 1068 Machine Learning: I. A Calibration Tool for Parameterization Improvement. *J.*
 1069 *Adv. Model. Earth Syst.*, 13(3), e2020MS002217. doi: 10.1029/2020MS002217
- 1070 Craig, P. D., & Banner, M. L. (1994). Modeling Wave-Enhanced Turbulence in the
 1071 Ocean Surface Layer. *J. Phys. Oceanogr.*, 24(12), 2546–2559. doi: 10.1175/
 1072 1520-0485(1994)024(2546:MWETIT)2.0.CO;2
- 1073 Cuxart, J., Bougeault, P., & Redelsperger, J.-L. (2000). A turbulence scheme allow-
 1074 ing for mesoscale and large-eddy simulations. *Quart. J. Roy. Meteorol. Soc.*,
 1075 126(562), 1–30. doi: 10.1002/qj.49712656202
- 1076 Deardorff, J. W. (1966). The Counter-Gradient Heat Flux in the Lower Atmosphere
 1077 and in the Laboratory. *J. Atmos. Sci.*, 23(5), 503–506. doi: 10.1175/1520-
 1078 -0469(1966)023(0503:TCGHFI)2.0.CO;2
- 1079 Deardorff, J. W. (1970). Convective Velocity and Temperature Scales for the Un-
 1080 stable Planetary Boundary Layer and for Rayleigh Convection. *J. Atmos. Sci.*,
 1081 27(8), 1211–1213. doi: 10.1175/1520-0469(1970)027(1211:CVATSF)2.0.CO;2
- 1082 Denbo, D. W., & Skyllingstad, E. D. (1996). An ocean large-eddy simulation model
 1083 with application to deep convection in the Greenland Sea. *J. Geophys. Res.*,
 1084 101(C1), 1095–1110. doi: 10.1029/95JC02828
- 1085 de Rooy, W. C., Bechtold, P., Fröhlich, K., Hohenegger, C., Jonker, H., Mironov,
 1086 D., ... Yano, J.-I. (2013). Entrainment and detrainment in cumulus con-
 1087 vection: an overview. *Quart. J. Roy. Meteorol. Soc.*, 139(670), 1–19. doi:
 1088 10.1002/qj.1959
- 1089 Eden, C. (2016). Closing the energy cycle in an ocean model. *Ocean Modell.*, 101,
 1090 30–42. doi: 10.1016/j.ocemod.2016.02.005
- 1091 Eden, C., & Olbers, D. (2014). An Energy Compartment Model for Propagation,
 1092 Nonlinear Interaction, and Dissipation of Internal Gravity Waves. *J. Phys.*
 1093 *Oceanogr.*, 44(8), 2093–2106. doi: 10.1175/JPO-D-13-0224.1
- 1094 Eldred, C., & Gay-Balmaz, F. (2021). Thermodynamically consistent semi-
 1095 compressible fluids: a variational perspective. *J. Phys. A Math. Theor.*, 54,
 1096 345701. doi: 10.1088/1751-8121/ac1384
- 1097 Evans, L. C. (2010). *Partial Differential Equations*. American Mathematical Soc.
- 1098 Fox-Kemper, B., Adcroft, A., Böning, C. W., Chassignet, E. P., Curchitser, E., Dan-
 1099 abasoglu, G., ... Yeager, S. G. (2019). Challenges and Prospects in Ocean
 1100 Circulation Models. *Front. Mar. Sci.*, 6, 65. doi: 10.3389/fmars.2019.00065
- 1101 Garanaik, A., Pereira, F. S., Smith, K., Robey, R., Li, Q., Pearson, B., &
 1102 Van Roekel, L. (2024). A New Hybrid Mass-Flux/High-Order Tur-
 1103 bulence Closure for Ocean Vertical Mixing. *Journal of Advances in*

- 1104 *Modeling Earth Systems*, 16(1). Retrieved 2024-01-31, from [https://](https://onlinelibrary.wiley.com/doi/abs/10.1029/2023MS003846)
 1105 onlinelibrary.wiley.com/doi/abs/10.1029/2023MS003846 (_eprint:
 1106 <https://onlinelibrary.wiley.com/doi/pdf/10.1029/2023MS003846>) doi:
 1107 10.1029/2023MS003846
- 1108 Garcia, J. R., & Mellado, J. P. (2014). The Two-Layer Structure of the Entrainment
 1109 Zone in the Convective Boundary Layer. *J. Atmos. Sci.*, 71(6), 1935–1955. doi:
 1110 10.1175/JAS-D-13-0148.1
- 1111 Garratt, J. (1994a). *The Atmospheric Boundary Layer*. Cambridge University
 1112 Press.
- 1113 Garratt, J. (1994b). Review: the atmospheric boundary layer. *Earth-Science Re-*
 1114 *views*, 37(1-2), 89–134. doi: 10.1016/0012-8252(94)90026-4
- 1115 Gaspar, P., Grégoris, Y., & Lefevre, J.-M. (1990). A simple eddy kinetic energy
 1116 model for simulations of the oceanic vertical mixing: Tests at station Papa and
 1117 long-term upper ocean study site. *J. Geophys. Res.*, 95(C9), 16179–16193. doi:
 1118 10.1029/JC095iC09p16179
- 1119 Giordani, H., Bourdallé-Badie, R., & Madec, G. (2020). An Eddy-Diffusivity Mass-
 1120 Flux Parameterization for Modeling Oceanic Convection. *J. Adv. Model. Earth*
 1121 *Syst.*, 12. doi: 10.1029/2020MS002078
- 1122 Gregory, D., Kershaw, R., & Inness, P. M. (1997). Parametrization of momen-
 1123 tum transport by convection. II: Tests in single-column and general circu-
 1124 lation models. *Quart. J. Roy. Meteorol. Soc.*, 123(541), 1153–1183. doi:
 1125 10.1002/qj.49712354103
- 1126 Haghshenas, A., & Mellado, J. P. (2019). Characterization of wind-shear effects on
 1127 entrainment in a convective boundary layer. *J. Fluid Mech.*, 858, 145–183. doi:
 1128 10.1017/jfm.2018.761
- 1129 Hahn, D. W., & Özişik, M. N. (2012). *Heat Conduction* (1st ed.). Wiley. doi: 10
 1130 .1002/9781118411285
- 1131 Han, J., & Bretherton, C. S. (2019). TKE-Based Moist Eddy-Diffusivity Mass-Flux
 1132 (EDMF) Parameterization for Vertical Turbulent Mixing. *Weather Forecast.*,
 1133 34(4), 869–886. doi: 10.1175/WAF-D-18-0146.1
- 1134 Higgins, C. W., Katul, G. G., Froidevaux, M., Simeonov, V., & Parlange, M. B.
 1135 (2013). Are atmospheric surface layer flows ergodic? *Geophys. Res. Lett.*,
 1136 40(12), 3342–3346.
- 1137 Holtslag, A. A. M., & Moeng, C.-H. (1991). Eddy diffusivity and countergradi-
 1138 ent transport in the convective atmospheric boundary layer. *J. Atmos. Sci.*,
 1139 48(14), 1690 - 1698. doi: [https://doi.org/10.1175/1520-0469\(1991\)048<1690:
 1140 EDACTI>2.0.CO;2](https://doi.org/10.1175/1520-0469(1991)048<1690:EDACTI>2.0.CO;2)
- 1141 Honnert, R., Couvreur, F., Masson, V., & Lancz, D. (2016). Sampling the Structure
 1142 of Convective Turbulence and Implications for Grey-Zone Parametrizations.
 1143 *Bound.-Lay. Meteorol.*, 160(1), 133–156. doi: 10.1007/s10546-016-0130-4
- 1144 Hourdin, F., Couvreur, F., & Menut, L. (2002). Parameterization of the Dry Con-
 1145 vective Boundary Layer Based on a Mass Flux Representation of Thermals.
 1146 *J. Atmos. Sci.*, 59(6), 1105–1123. doi: 10.1175/1520-0469(2002)059<1105:
 1147 POTDCB>2.0.CO;2
- 1148 Hourdin, F., Mauritsen, T., Gettelman, A., Golaz, J.-C., Balaji, V., Duan, Q., ...
 1149 Williamson, D. (2017). The Art and Science of Climate Model Tuning. *Bull.*
 1150 *Amer. Meteor. Soc.*, 98(3), 589–602. doi: 10.1175/BAMS-D-15-00135.1
- 1151 Jansen, M. F., Adcroft, A., Khani, S., & Kong, H. (2019). Toward an Energetically
 1152 Consistent, Resolution Aware Parameterization of Ocean Mesoscale Eddies. *J.*
 1153 *Adv. Model. Earth Syst.*, 11(8), 2844–2860. doi: 10.1029/2019MS001750
- 1154 Johansson, C., Smedman, A.-S., Höglström, U., Brousseau, J. G., & Khanna, S.
 1155 (2001). Critical Test of the Validity of Monin–Obukhov Similarity dur-
 1156 ing Convective Conditions. *J. Atmos. Sci.*, 58(12), 1549–1566. doi:
 1157 10.1175/1520-0469(2001)058<1549:CTOTVO>2.0.CO;2
- 1158 Kato, H., & Phillips, O. M. (1969). On the penetration of a turbulent layer

- 1159 into stratified fluid. *J. Fluid Mech.*, *37*(4), 643–655. doi: 10.1017/
 1160 S0022112069000784
- 1161 Lac, C., Chaboureaud, J.-P., Masson, V., Pinty, J.-P., Tulet, P., Escobar, J., ...
 1162 Wautelet, P. (2018). Overview of the Meso-NH model version 5.4 and
 1163 its applications. *Geosci. Model Dev.*, *11*(5), 1929–1969. doi: 10.5194/
 1164 gmd-11-1929-2018
- 1165 Large, W. G., McWilliams, J. C., & Doney, S. C. (1994). Oceanic vertical mixing:
 1166 A review and a model with a nonlocal boundary layer parameterization. *Rev.*
 1167 *Geophys.*, *32*(4), 363–403. doi: 10.1029/94RG01872
- 1168 Lauritzen, P. H., Kevlahan, N. K.-R., Toniazzo, T., Eldred, C., Dubos, T.,
 1169 Gassmann, A., ... Bacmeister, J. T. (2022). Reconciling and Improving
 1170 Formulations for Thermodynamics and Conservation Principles in Earth Sys-
 1171 tem Models (ESMs). *J. Adv. Model. Earth Syst.*, *14*(9), e2022MS003117. doi:
 1172 10.1029/2022MS003117
- 1173 Legay, A., Deremble, B., Penduff, T., Brasseur, P., & Molines, J.-M. (2023). A
 1174 generic framework for evaluating the oceanic mixed layer depth dynamics
 1175 (preprint). Preprints. doi: 10.22541/essoar.168563421.17506622/v1
- 1176 LeVeque, R. J. (2002). *Finite volume methods for hyperbolic problems* (Vol. 31).
 1177 Cambridge university press.
- 1178 Li, Q., Cheng, Y., & Gentine, P. (2021). Connection Between Mass Flux Trans-
 1179 port and Eddy Diffusivity in Convective Atmospheric Boundary Layers. *Geo-*
 1180 *phys. Res. Lett.*, *48*(8), e2020GL092073. doi: 10.1029/2020GL092073
- 1181 Li, Q., Gentine, P., Mellado, J. P., & McColl, K. A. (2018). Implications of Nonlocal
 1182 Transport and Conditionally Averaged Statistics on Monin–Obukhov Similar-
 1183 ity Theory and Townsend’s Attached Eddy Hypothesis. *J. Atmos. Sci.*, *75*(10),
 1184 3403–3431. doi: 10.1175/JAS-D-17-0301.1
- 1185 Madec, G., Bourdallé-Badie, R., Chanut, J., Clementi, E., Coward, A., Ethé,
 1186 C., ... Samson, G. (2019). *NEMO ocean engine*. Retrieved from
 1187 <https://zenodo.org/record/1464816> doi: 10.5281/ZENODO.1464816
- 1188 Madec, G., Delecluse, P., Crepon, M., & Chartier, M. (1991). A Three-
 1189 Dimensional Numerical Study of Deep-Water Formation in the North-
 1190 western Mediterranean Sea. *J. Phys. Oceanogr.*, *21*(9), 1349–1371. doi:
 1191 10.1175/1520-0485(1991)021<1349:ATDNSO>2.0.CO;2
- 1192 Marshall, J., Hill, C., Perelman, L., & Adcroft, A. (1997). Hydrostatic, quasi-
 1193 hydrostatic, and nonhydrostatic ocean modeling. *J. Geophys. Res.*, *102*(C3),
 1194 5733–5752. doi: 10.1029/96JC02776
- 1195 Marshall, J., & Schott, F. (1999). Open-ocean convection: Observations, theory, and
 1196 models. *Rev. Geophys.*, *37*(1), 1–64. doi: 10.1029/98RG02739
- 1197 Martin, T., Park, W., & Latif, M. (2013). Multi-centennial variability controlled by
 1198 Southern Ocean convection in the Kiel Climate Model. *Clim. Dynam.*, *40*(7),
 1199 2005–2022. doi: 10.1007/s00382-012-1586-7
- 1200 McDougall, T. J. (2003). Potential Enthalpy: A Conservative Oceanic Variable for
 1201 Evaluating Heat Content and Heat Fluxes. *J. Phys. Oceanogr.*, *33*(5), 945–963.
 1202 doi: 10.1175/1520-0485(2003)033<0945:PEACOV>2.0.CO;2
- 1203 Mellor, G. (1973). Analytic Prediction of the Properties of Stratified Planetary Sur-
 1204 face Layers. *J. Atmos. Sci.*, *30*(6), 1061–1069. doi: 10.1175/1520-0469(1973)
 1205 030<1061:APOTPO>2.0.CO;2
- 1206 Mellor, G., & Blumberg, A. (2004). Wave Breaking and Ocean Surface Layer Ther-
 1207 mal Response. *J. Phys. Oceanogr.*, *34*(3), 693–698. doi: 10.1175/2517.1
- 1208 Moore, G. W. K., Våge, K., Pickart, R. S., & Renfrew, I. A. (2015). Decreasing in-
 1209 tensity of open-ocean convection in the Greenland and Iceland seas. *Nat. Clim.*
 1210 *Change*, *5*(9), 877–882. doi: 10.1038/nclimate2688
- 1211 Obukhov, A. M. (1971). Turbulence in an atmosphere with a non-uniform tempera-
 1212 ture. *Bound.-Lay. Meteorol.*, *2*(1), 7–29. doi: 10.1007/BF00718085
- 1213 Olbers, D., Willebrand, J., & Eden, C. (2012). *Ocean Dynamics*. Berlin, Heidelberg:

- 1214 Springer Berlin Heidelberg. doi: 10.1007/978-3-642-23450-7
- 1215 Pauluis, O. (2008). Thermodynamic Consistency of the Anelastic Approx-
 1216 imation for a Moist Atmosphere. *J. Atmos. Sci.*, *65*, 2719–2729. doi:
 1217 10.1175/2007JAS2475.1
- 1218 Pergaud, J., Masson, V., Malardel, S., & Couvreux, F. (2009). A Parameterization
 1219 of Dry Thermals and Shallow Cumuli for Mesoscale Numerical Weather Pre-
 1220 diction. *Bound.-Lay. Meteorol.*, *132*, 83–106. doi: 10.1007/s10546-009-9388-0
- 1221 Peterson, P. (2009). F2PY: a tool for connecting Fortran and Python programs. *Int.*
 1222 *j. comput. sci. eng.*, *4*(4), 296. doi: 10.1504/IJCSE.2009.029165
- 1223 Piron, A., Thierry, V., Mercier, H., & Caniaux, G. (2016). Argo float observations of
 1224 basin-scale deep convection in the Irminger sea during winter 2011–2012. *Deep-*
 1225 *Sea Res. I*, *109*, 76–90. doi: 10.1016/j.dsr.2015.12.012
- 1226 Pope, S. B. (2004). Ten questions concerning the large-eddy simulation of turbulent
 1227 flows. *New J. Phys.*, *6*, 35–35. doi: 10.1088/1367-2630/6/1/035
- 1228 Ramadhan, A., Wagner, G. L., Hill, C., Campin, J.-M., Churavy, V., Besard, T.,
 1229 ... Marshall, J. (2020). Oceananigans.jl: Fast and friendly geophysical fluid
 1230 dynamics on GPUs. *Journal of Open Source Software*, *5*(53), 2018. Retrieved
 1231 from <https://doi.org/10.21105/joss.02018> doi: 10.21105/joss.02018
- 1232 Resseguier, V., Mémin, E., & Chapron, B. (2017). Geophysical flows under location
 1233 uncertainty, Part II Quasi-geostrophy and efficient ensemble spreading. *Geo-*
 1234 *phys. Astrophys. Fluid Dyn.*, *111*(3), 177–208.
- 1235 Rio, C., Hourdin, F., Couvreux, F., & Jam, A. (2010). Resolved Versus
 1236 Parametrized Boundary-Layer Plumes. Part II: Continuous Formulations of
 1237 Mixing Rates for Mass-Flux Schemes. *Bound.-Lay. Meteorol.*, *135*(3), 469–483.
 1238 doi: 10.1007/s10546-010-9478-z
- 1239 Roode, S. R. d., Siebesma, A. P., Jonker, H. J. J., & Voogd, Y. d. (2012). Parame-
 1240 terization of the Vertical Velocity Equation for Shallow Cumulus Clouds. *Mon.*
 1241 *Weather Rev.*, *140*(8), 2424–2436. doi: 10.1175/MWR-D-11-00277.1
- 1242 Rotunno, R., & Klemp, J. B. (1982). The Influence of the Shear-Induced Pressure
 1243 Gradient on Thunderstorm Motion. *Mon. Weather Rev.*, *110*(2), 136–151. doi:
 1244 10.1175/1520-0493(1982)110<0136:TIOTSI>2.0.CO;2
- 1245 Schmidt, H., & Schumann, U. (1989). Coherent structure of the convective boundary
 1246 layer derived from large-eddy simulations. *J. Fluid Mech.*, *200*, 511–562. doi:
 1247 10.1017/S0022112089000753
- 1248 Schmitt, F. G. (2007). About Boussinesq’s turbulent viscosity hypothesis: histori-
 1249 cal remarks and a direct evaluation of its validity. *Comptes Rendus Mécanique*,
 1250 *335*(9), 617–627. doi: 10.1016/j.crme.2007.08.004
- 1251 Schneider, T., Teixeira, J., Bretherton, C. S., Brient, F., Pressel, K. G., Schär, C.,
 1252 & Siebesma, A. P. (2017). Climate goals and computing the future of clouds.
 1253 *Nat. Clim. Change*, *7*(1), 3–5. doi: 10.1038/nclimate3190
- 1254 Siebesma, A. P., Soares, P. M. M., & Teixeira, J. (2007). A Combined Eddy-
 1255 Diffusivity Mass-Flux Approach for the Convective Boundary Layer. *J. Atmos.*
 1256 *Sci.*, *64*(4), 1230–1248. doi: 10.1175/JAS3888.1
- 1257 Soares, P. M. M., Miranda, P. M. A., Siebesma, A. P., & Teixeira, J. (2004).
 1258 An eddy-diffusivity/mass-flux parametrization for dry and shallow cumu-
 1259 lus convection. *Quart. J. Roy. Meteorol. Soc.*, *130*(604), 3365–3383. doi:
 1260 10.1256/qj.03.223
- 1261 Souza, A. N., Wagner, G. L., Ramadhan, A., Allen, B., Churavy, V., Schloss, J., ...
 1262 Ferrari, R. (2020). Uncertainty Quantification of Ocean Parameterizations:
 1263 Application to the K-Profile-Parameterization for Penetrative Convection. *J.*
 1264 *Adv. Model. Earth Syst.*, *12*(12). doi: 10.1029/2020MS002108
- 1265 Tailleux, R. (2012). Thermodynamics/Dynamics Coupling in Weakly Compressible
 1266 Turbulent Stratified Fluids. *International Scholarly Research Notices*, *2012*,
 1267 e609701. (Publisher: Hindawi) doi: 10.5402/2012/609701
- 1268 Tailleux, R., & Dubos, T. (2023). *A Simple and Transparent Method for Im-*

- 1269 *proving the Energetics and Thermodynamics of Seawater Approximations:*
 1270 *Static Energy Asymptotics (SEA).* arXiv. (arXiv:2311.11387 [physics]) doi:
 1271 10.48550/arXiv.2311.11387
- 1272 Tan, Z., Kaul, C. M., Pressel, K. G., Cohen, Y., Schneider, T., & Teixeira, J. (2018).
 1273 An Extended Eddy-Diffusivity Mass-Flux Scheme for Unified Representation of
 1274 Subgrid-Scale Turbulence and Convection. *J. Adv. Model. Earth Syst.*, *10*(3),
 1275 770–800. doi: 10.1002/2017MS001162
- 1276 Thuburn, J., Weller, H., Vallis, G. K., Beare, R. J., & Whittall, M. (2018). A
 1277 Framework for Convection and Boundary Layer Parameterization De-
 1278 rived from Conditional Filtering. *J. Atmos. Sci.*, *75*(3), 965–981. doi:
 1279 10.1175/JAS-D-17-0130.1
- 1280 Troen, I. B., & Mahrt, L. (1986). A simple model of the atmospheric boundary
 1281 layer; sensitivity to surface evaporation. *Bound.-Lay. Meteorol.*, *37*(1), 129–
 1282 148. doi: 10.1007/BF00122760
- 1283 Turner, J. S. (1979). *Buoyancy Effects in Fluids*. Cambridge University Press.
- 1284 Vallis, G. K. (2017). *Atmospheric and oceanic fluid dynamics*. Cambridge University
 1285 Press.
- 1286 Van Roekel, L., Adcroft, A. J., Danabasoglu, G., Griffies, S. M., Kauffman, B.,
 1287 Large, W., . . . Schmidt, M. (2018). The KPP Boundary Layer Scheme for
 1288 the Ocean: Revisiting Its Formulation and Benchmarking One-Dimensional
 1289 Simulations Relative to LES. *J. Adv. Model. Earth Syst.*, *10*(11), 2647–2685.
 1290 doi: 10.1029/2018MS001336
- 1291 Waldman, R., Somot, S., Herrmann, M., Bosse, A., Caniaux, G., Estournel, C.,
 1292 . . . Testor, P. (2017). Modeling the intense 2012–2013 dense water for-
 1293 mation event in the northwestern mediterranean sea: Evaluation with an
 1294 ensemble simulation approach. *J. Geophys. Res.*, *122*(2), 1297–1324. doi:
 1295 <https://doi.org/10.1002/2016JC012437>
- 1296 Witek, M. L., Teixeira, J., & Matheou, G. (2011a). An Eddy Diffusivity–Mass
 1297 Flux Approach to the Vertical Transport of Turbulent Kinetic Energy in
 1298 Convective Boundary Layers. *J. Atmos. Sci.*, *68*(10), 2385–2394. doi:
 1299 10.1175/JAS-D-11-06.1
- 1300 Witek, M. L., Teixeira, J., & Matheou, G. (2011b). An Integrated TKE-Based Eddy
 1301 Diffusivity/Mass Flux Boundary Layer Closure for the Dry Convective Bound-
 1302 ary Layer. *J. Atmos. Sci.*, *68*(7), 1526–1540. doi: 10.1175/2011JAS3548.1
- 1303 Wu, X., & Yanai, M. (1994). Effects of Vertical Wind Shear on the Cumu-
 1304 lus Transport of Momentum: Observations and Parameterization. *J. At-
 1305 mos. Sci.*, *51*(12), 1640–1660. doi: 10.1175/1520-0469(1994)051<1640:
 1306 EOVSWSO>2.0.CO;2
- 1307 Wyngaard, J. C., & Coté, O. R. (1971). The Budgets of Turbulent Kinetic Energy
 1308 and Temperature Variance in the Atmospheric Surface Layer. *J. Atmos. Sci.*,
 1309 *28*(2), 190–201. doi: 10.1175/1520-0469(1971)028<0190:TBOTKE>2.0.CO;2
- 1310 Yano, J.-I. (2014). Formulation structure of the mass-flux convection parameteri-
 1311 zation. *Dynam. Atmos. Oceans*, *67*, 1–28. doi: 10.1016/j.dynatmoce.2014.04
 1312 .002
- 1313 Young, W. R. (2010). Dynamic Enthalpy, Conservative Temperature, and the Sea-
 1314 water Boussinesq Approximation. *J. Phys. Oceanogr.*, *40*(2), 394–400. doi: 10
 1315 .1175/2009JPO4294.1
- 1316 Zhang, M., Somerville, R. C. J., & Xie, S. (2016, April). The SCM Concept and
 1317 Creation of ARM Forcing Datasets. *Meteorol. Monogr.*, *57*(1), 24.1–24.12. doi:
 1318 10.1175/AMSMONOGRAPHIS-D-15-0040.1
- 1319 Zheng, Z., Harcourt, R. R., & D’Asaro, E. A. (2021). Evaluating Monin–Obukhov
 1320 Scaling in the Unstable Oceanic Surface Layer. *J. Phys. Oceanogr.*, *51*(3), 911–
 1321 930. doi: 10.1175/JPO-D-20-0201.1